Catena 247 (2024) 108509

Contents lists available at ScienceDirect

Catena

journal homepage: www.elsevier.com/locate/catena

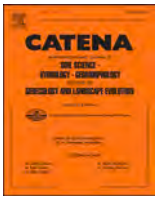

Geotechnical and geophysical property models of soil-covered slopes prone to landsliding. The case study of the Ischia Island (southern Italy)

R. Di Maio [a], R. Salone [a], C. De Paola [a,b], R. Carbonari [c], D. Cusano [a], P. De Vita [a,*]

[a] Dipartimento di Scienze della Terra, dell'Ambiente e delle Risorse, Università di Napoli Federico II, 80126, Naples, Italy
[b] Istituto Nazionale di Geofisica e Vulcanologia, Osservatorio Vesuviano, 80124, Naples, Italy
[c] Institute of Earth Sciences, The Hebrew University of Jerusalem, 9190401, Jerusalem, Israel

ARTICLE INFO

Keywords:
Rainfall-induced shallow landslides
Soil cover
Engineering geological modeling
Geophysical prospecting
Geotechnical and geophysical properties
Landslide hazard assessment
LEWS

ABSTRACT

The physical and geotechnical characterization of surficial geological systems forming slopes and the definition of soil hydrological conditions leading to rainfall-induced shallow landslides are key factors for the effective landslide hazard assessment and setting of Landslide Early Warning Systems (LEWS). Indeed, poor knowledge of the thicknesses, local stratigraphic features and geotechnical properties of soil/regolith coverings, as well as their soil hydrological status, can lead to oversimplified assumptions resulting in high uncertainties in the prediction of landslide hazard in space and time. This work proposes the integration of geotechnical and geophysical approaches to advance the reconstruction of surficial engineering geological models and the assessment of the hydrological status of soil-covered slopes prone to landsliding, to be used for the setting of physical-based slope models. A combined field and laboratory geotechnical and geophysical study of a sector of Mount di Vezzi (Ischia Island, southern Italy), known for the recurrent shallow rainfall-induced landslides affecting settlements in the foothills, was carried out to test our approach. As a principal result, the integration of both approaches advances the reconstruction of a comprehensive physical model of the potentially unstable slopes. Significantly, the coupling of geophysical and geotechnical properties, such as electrical resistivity, volumetric water content and soil water pressure head, allows the use of resistivity as a proxy for the hydrological status of the soil mantled slopes at a volume scale consistent with that of the initial stage of shallow landslides, ranging from 10^1 to 10^3 m^3. The results obtained are expected to be applicable for the definition of the parameters of physical-based slope models to be used for supporting LEWS, built on rainfall thresholds and hydrological measurements, thus for the estimation of the spatial and temporal variation of shallow rainfall-induced landslide hazard.

1. Introduction

The engineering geological and hydrological characterization of soil-covered slopes potentially prone to rainfall-induced shallow landslides is essential for the effective setting of physical-based models aimed at the hazard assessment through Landslide Early Warning Systems (LEWS) (Borga et al., 1998; Dietrich and Montgomery, 1998; Lu and Godt, 2008; Simoni et al., 2008; Baum and Godt, 2010; Ren et al., 2010; Arnone et al., 2011; Salciarini et al., 2012, 2017; Park et al., 2013; Rossi et al., 2013; Chen and Zhang, 2014). Physical-based slope models consider both static and dynamic variables (Napolitano et al., 2016; Salvatici et al., 2018; Forte et al., 2019; Tufano et al., 2021). The first, such as stratigraphic, geotechnical and morphological settings, control the triggering of landslides in space. Instead, the second ones, such as the soil hydrological status, determine the landslide occurrence in time. Therefore, the knowledge of local stratigraphic features and thickness of the soil/regolith coverings, geotechnical characterization and soil hydrological conditions are key factors to avoid oversimplified assumptions of physical-based slope models aimed at spatial and temporal landslide hazard assessment. This means that high-quality physical and geotechnical datasets are required to reconstruct reliable physical-based models of rainfall-induced shallow landslides. Indeed, poor knowledge of soil hydrological and geotechnical parameters and their spatial distribution can lead to high uncertainties in the model output and thus to low accuracy in predicting spatial and temporal occurrence of landslides (e.g. Tofani et al., 2017; Prancevic et al., 2020; Pirone et al., 2023).

Currently, the parameters of physical-based models of slopes potentially prone to shallow landslides are essentially determined by

* Corresponding author.
E-mail address: padevita@unina.it (P. De Vita).

https://doi.org/10.1016/j.catena.2024.108509
Received 26 March 2024; Received in revised form 30 September 2024; Accepted 25 October 2024
Available online 16 November 2024

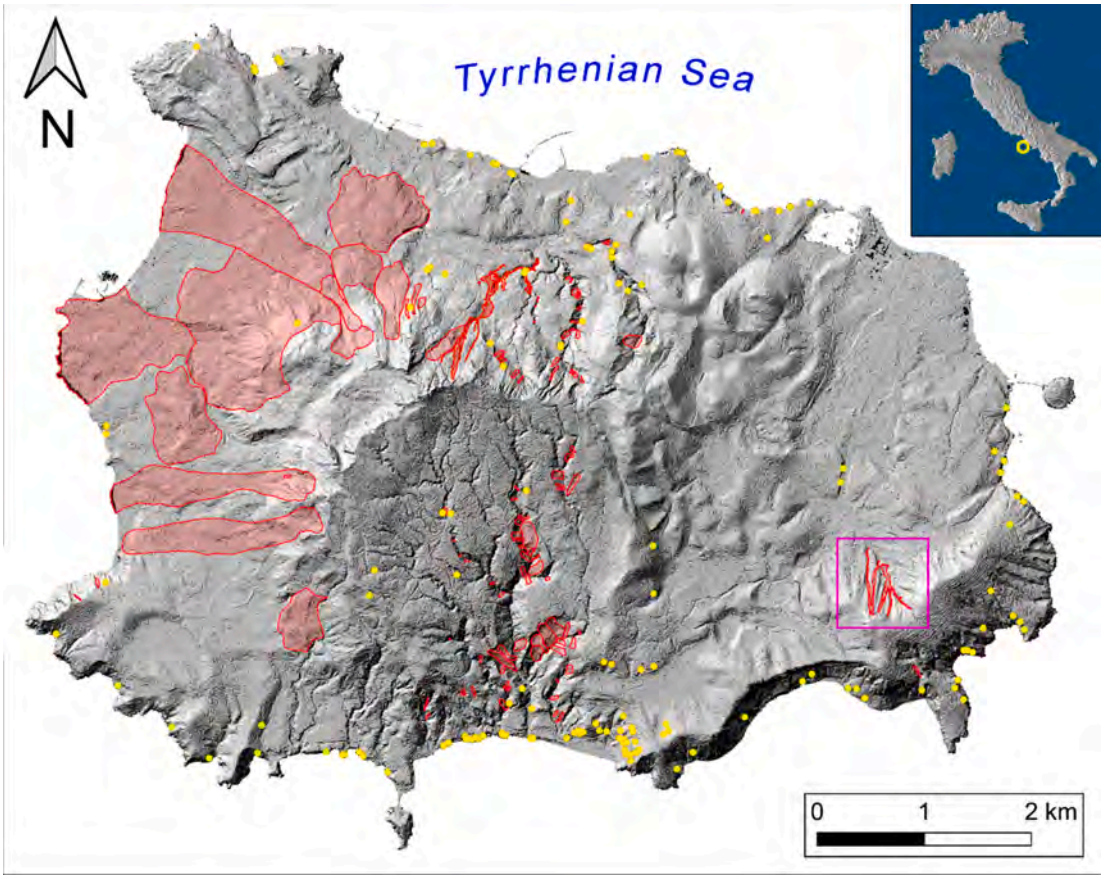

Fig. 1. High-resolution hillshade of the Ischia Island with an inventory of landslide phenomena (Fusco et al., 2023). Key to symbols: red polygons) larger landslides; yellow dots) punctual landslides. The location of the study area at Mount di Vezzi is represented by the purple rectangle (zoomed in Fig. 2).

integrating basic morphological data (slope angle) and sparse geotechnical investigations, as well as sporadic and localized soil hydrological monitoring. All these types of field investigations consist of site-specific measurements or sampling, which generally investigate soil volumes in the order of $10^{-3} – 10^{-1}$ m^3. They can therefore hardly capture the spatial variability and heterogeneity of geotechnical and hydrological soil properties (Baecher and Christian, 2003) on a scale corresponding to that of landslide phenomena, which extends over volumes several orders of magnitude larger ($10^2 – 10^6$ m^3).

In contrast, geophysical prospecting can define the buried stratigraphic setting and its physical properties over an underground volume that is more representative of the hydrological conditions controlling slope instability due to surface measurements carried out over large areas. A comprehensive review of the geophysical investigation of landslide areas was given by Jongmans and Garambois (2007). Although the authors highlighted the advantages of the most widely used geophysical techniques in this application field, such as seismic refraction, electrical resistivity tomography, passive seismic and ground penetrating radar, they also provided a critical analysis of their limitations. These were mainly attributed to shortcomings in discussing the resolution and penetration depth of each method, in critically explaining the geological interpretation of geophysical data, and in achieving quantitative information from geophysics in terms of geotechnical parameters and hydrological properties. Subsequently, based on this review, Pazzi et al. (2019) analysed papers published between 2007 and 2018, with the main objective of demonstrating the efforts made by the geophysical community to overcome the limitations highlighted by Jongmans and Garambois (2007). Due to recent advances in geophysical technologies and data processing methods, Pazzi et al. (2019) highlighted in their review significant improvements in the geological interpretation of geophysical data and in the resolution of the applied methods. Indeed, various successful examples of the integrated use of geotechnical and geophysical data for the study of areas affected by landslide phenomena have been published in recent years (e.g. Zarroca et al., 2014; Crawford et al., 2015; Giocoli et al., 2015; Crawford and Bryson, 2018; Pasierb et al., 2019; Khan et al., 2021; Kiernan et al., 2022). Conversely, the analysis of previous studies revealed very few efforts to establish quantitative relationships between geophysical data and geotechnical/hydrological parameters. The present paper aims to contribute to this issue by developing an integrated approach, based on geophysical and geotechnical field and laboratory investigations, which is expected to advance the characterization of slope areas potentially prone to shallow rainfall-induced landslides. The proposed procedure has been tested on a slope area located on the Ischia Island (Campania, southern Italy), well known from chronicles for the recurrent deadly landslides that hit settlements located at the footslopes. In particular, a joint analysis of in-situ and laboratory geotechnical and geophysical data was carried out to obtain a detailed characterization of the stratigraphic, physical and hydrological conditions of the pyroclastic deposits on Mount di Vezzi (Ischia Island, southern Italy), from which five debris flows (Figs. 1, 2 and 3) initiated on 30 April 2006 causing the loss of four human lives. An integrated analysis of the investigated geophysical and geotechnical parameters was also performed to establish a possible empirical relationship between resistivity and soil hydrological variables, such as effective saturation and soil water pressure head. This could allow the use of the geoelectrical monitoring to estimate the hydrological status of the soil cover at the slope scale, which is a key factor in the setting of effective LEWS based on hydrological measurements.

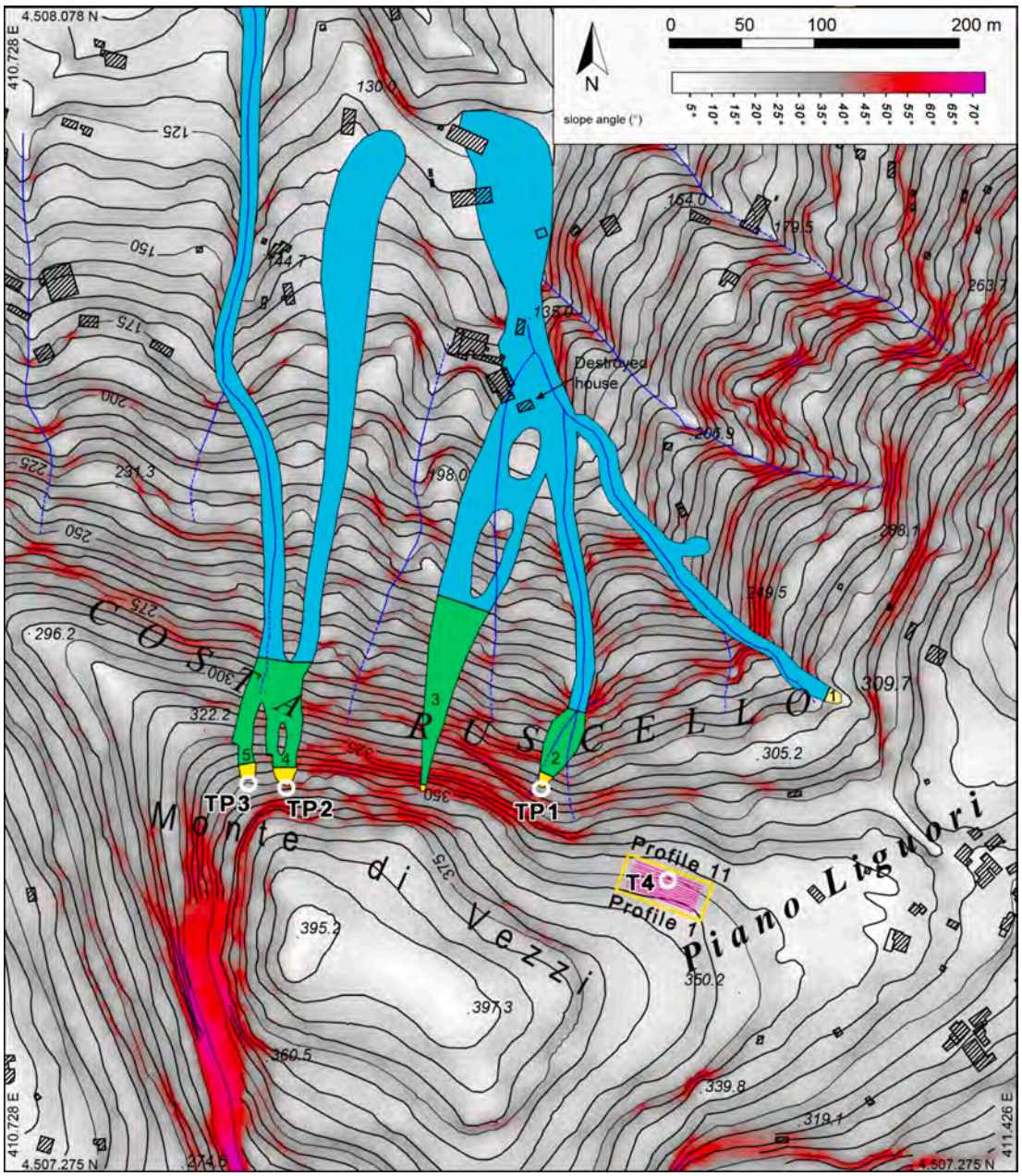

Fig. 2. Landslides of April 30, 2006 on Mount di Vezzi (see Fig. 1). The five landslides were numbered from East to West. The shading indicates the slope angle (red above 40°). The colors in the landslide areas correspond to the type of landslide mechanisms (Cruden and Varnes, 1996; Hungr et al., 2014): yellow) debris slide; green) debris avalanche; cyan) debris flow. Location of test pits and joined dynamic penetrometer tests (TP1, TP2 and TP3) are shown in the surrounding of the landslide source area. 11 ERT, SP geophysical investigations and test pit T4 used for soil sampling were carried out in a nearby area (see Fig. 3) represented by the yellow rectangle. The valleyward path of landslide No. 5 is truncated due its continuation in the hydrographic channel as a hyperconcentrated flow, thus in form of a flood phenomenon. Coordinates are in UTM WGS84 system (Fuse 33).

2. Study area and landslide description

The Ischia Island, located in the north-western sector of the Gulf of Naples (Fig. 1), is characterized by very complex geological features consisting of volcanic series and structures covered by diffuse marine and continental deposits. The geological complexity of the Island is due to the alternation of phases of construction of the volcanic structure, initiated before 150 k-years ago, and dismantling, caused by the interaction of volcano-tectonic phenomena and slope instability (de Vita et al., 2006; 2010; Della Seta et al., 2012; 2015; Marmoni et al., 2017).

The most important reliefs of the island are Mt. Epomeo (787 m a.s.l.), formed by a resurgent block in a large green tuff caldera (Selva et al., 2019), and Mount di Vezzi (392 m a.s.l.), formed by a 150 m thick lava dome (Vezzoli, 1988), which controls the morpho-structural setting of the mountain. The latter is formed, from the bottom, by the "Scarrupata di Barano" Formation, constituted by tuffs and tuff-breccias with ash-fall pumices and alcalitrachitic lavas, the Pignatiello Formation, constituted by very thick strata of lapilli, pumiceous ash-fall breccias, unwelded ash-flow and pumice-flow deposit, belonging to the Green Tuff of the Mount Epomeo Formation, and finally the Piano Liguori Formation, constituted by light colored ash with intercalated pumiceous lapilli levels (Chiesa et al., 1987; Vezzoli, 1988). In addition, abundant detrital deposits are widespread in the area, mostly derived from landslide processes developed along the volcanic slopes (Mele and Del Prete, 1998). The climate features are typically Mediterranean with humid winter and dry and hot summer and classifiable as "hot dry-summer" (Csa) (Beck et al., 2018),

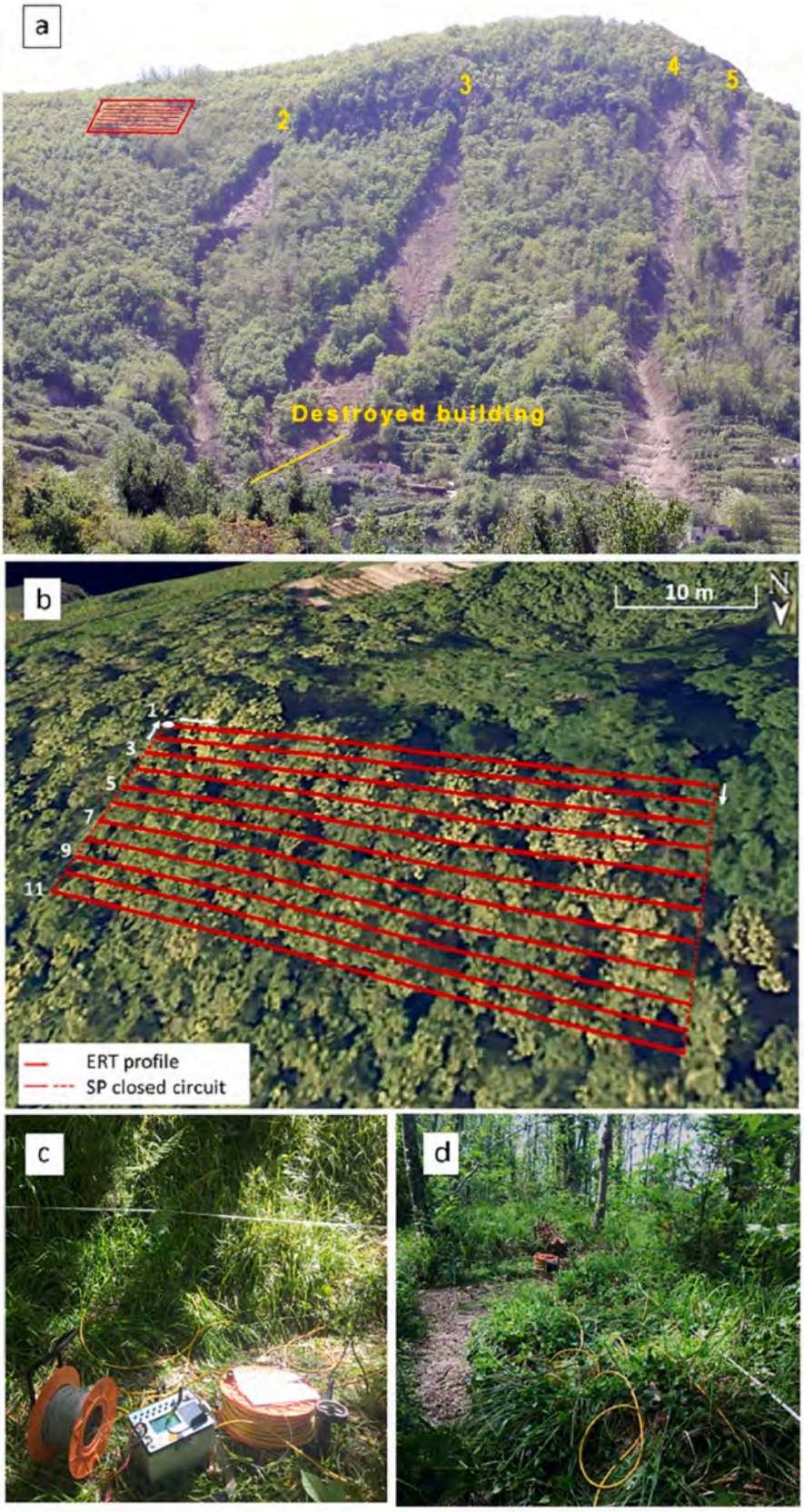

Fig. 3. (a) Frontal view of Mount Di Vezzi northern slope with landslides of 30 April 2006 (No. 2, 3, 4 and 5 in Fig. 2; No. 1 is not visible from this point of view) and approximate location of the geophysical survey (red rectangle, see Fig. 2). (b) Distribution of the 11 ERT profiles; the continuous and dashed red lines represent the closed loop where the SP measurements were taken, while the white arrowheads and the white dot on profile 1 indicate the path of the SP measurements and the final reference point of the entire SP dataset, respectively (Barde-Cabusson et al., 2021). (c) Photograph of the IRIS-SYSCAL PRO georesistivimeter equipped with two multi-electrode cables (yellow wires in c and d) of 24 electrodes each spaced 1 m apart.

with mean annual precipitation of about 820 mm and mean annual air temperature of 15.5 °C. The predominant land cover type occurring in landslides sources areas is chestnut deciduous forest (*Castanea Sativa*).

Due to the high relief energy, the Ischia Island has been recurrently affected by landslides induced by heavy rainfall events and earthquakes, as indicated by previous studies (Mele and Del Prete, 1998; Fusco et al., 2023), which recognized 240 landslide phenomena on the Island since historical times. These phenomena have varied from shallow debris slides evolving in flow-like types (debris flows and hyperconcentrated flows) with high catastrophic effects (Santo et al., 2012), involving pyroclastic and pedogenized soil coverings, to rockfalls of tuff and lava from steep slopes of coastal cliffs or fault scarps (Del Prete and Mele, 1999; 2006; Alvioli, 2022; Massaro et al., 2024). Flow-like phenomena, occurring during intense thunderstorms, caused the repeated flooding of the urbanized areas of Casamicciola, Lacco Ameno, Maronti and Monterone (Forio), determining the greatest damage and loss of human lives since 1910 (Donzelli, 1910; Bordiga, 1914) and totaling 42 up to 2022.

Among the most important landslide events in recent decades are the debris slide – debris flows (Cruden and Varnes, 1996; Hungr et al., 2014) that occurred in January 1997, July 1999, September 2001, April 2006, November 2009, November 2022 (de Riso et al., 2004; De Vita et al., 2007; Santo et al., 2012; Romeo et al., 2023) involving from 5×10^3 m^3 to 50×10^3 m^3 of pyroclastic, marine sedimentary and pedogenized materials, as well as wooded vegetation cover, with a very rapid and catastrophic kinematics and causing the loss of 4 (2006), 1 (2009) and 12 (2022) casualties.

Regarding the study area, on April 30, 2006, in the early hours of the morning, five shallow debris slides were triggered on the northern side of the Mount di Vezzi, which moved down the slope as very rapid flow-like landslides, channeling into the hydrographic network and reaching the footslope. One of the landslides hit and destroyed a building located at the outlet of a channel, causing the loss of four human lives. The landslides were recognized as shallow slope movements, involving the loose pyroclastic soils covering the volcanic bedrock with an average depth less than one meter. Furthermore, the landslides appeared to be complex in style and, according to the grain size of the depleted soils, classifiable as debris slides-debris flows with an intermediate phase of debris-avalanches (Cruden and Varnes, 1996; Hungr et al., 2014). The landslides were preliminarily studied by field investigations consisting of topographic, stratigraphic, geotechnical tests and resistivity surveys (De Vita et al, 2007; Di Maio et al., 2007). The main results were the recognition of a rotational kinematics of the initial debris slides involving very loose and permeable surficial ash-fall pyroclastic deposits overlapping a fine ash pyroclastic soil with higher compaction grade and lower permeability. Based on these characteristics, the landslides that occurred on Mount di Vezzi on April 30, 2006, can be considered analogous to the numerous other cases that have occurred along the *peri*-vesuvian carbonate slopes (De Vita et al., 2013; Napolitano et al., 2016; Fusco et al., 2021; Sepe et al., 2023).

3. Materials and methods

The proposed integrated approach consists of two phases related to in-situ and laboratory measurements of geotechnical and geophysical parameters whose combination allowed a comprehensive characterization of the investigated test site at the slope scale. Due to difficult operating conditions caused by high slope angles ranging from 35° to 50° and dense wood vegetation, only part of the field engineering geological investigations was carried out directly in the landslide source areas, which consisted of 3 test pits joined with dynamic penetrometer tests (TP1, TP2 and TP3 in Fig. 2). Instead, geophysical investigations, consisting of electrical resistivity tomography (ERT) and self-potential (SP) surveys, jointly with geotechnical surveys, were carried out laterally to the landslide source areas at a site located about 100 m eastward, with a lower slope angle (30°) and scarce wood vegetation (Fig. 2), therefore favorable for the correct deployment of electrical cables.

As demonstrated by the observation of stratigraphic features, this site was recognized as equivalent to the landslide source areas in terms of the soil horizons involved in landsliding. At the same site, 3 sets of undisturbed soil samples were collected by a test pit and analyzed using both laboratory geotechnical and geophysical methods (T4 in Fig. 2). The combined geotechnical and geophysical field survey of the test site was conducted in May 2017.

3.1. Engineering geological characterization of landslide materials

3.1.1. Geotechnical field testing

The surficial deposits involved in the landslides that occurred on April 30, 2006, on Mount di Vezzi were investigated by a stratigraphic characterization of outcrops corresponding to the main scarps and flanks of landslides, road cuts and test pits manually dug. Specifically, a criterion based on the nomenclature of pedologic soil horizons was applied (Soil Science Division Staff, 2017; USDA, 2022).

Natural cuts and outcrops, as well as 3 test pits, allowed the observation of approximately the first 3 m of the soil pyroclastic mantle, measured along the vertical (apparent thickness), in landslide source areas. To extend the information obtained from the stratigraphic surveys to a greater depth and to indicatively characterize the mechanical properties of the soil cover overlying the bedrock, 3 dynamic penetrometer tests were carried out for each test pit location. A dynamic penetrometer specifically designed to be easily transported under difficult operating conditions was used. This consists of a 6 kg beating mass (m) falling from a height of 0.5 m (H) onto an anvil (m') of 3.2 kg; the latter is connected to a 16 mm diameter rod series (1.58 kg/m), at the bottom of which is a standard tip (CENT/TC 341 N 119 E, 2003) with a 6×10^{-4} m^2 area (A). The total energy developed by the falling mass is 29.43 J (m × H × g). The soil shear strength can be appraised, starting from the number of blows (N_z) required to penetrate the depth interval (z), using the penetration resistance (R) expressed by the "Dutch Formula" (Sanglerat, 1972; Cassan, 1988):

$$R[Pa] = \frac{m \times H \times g}{A \times \frac{z}{N_z}} \times \frac{m}{m + m'} \tag{1}$$

The value of the penetration interval (z) at which the dynamic strength was discretized is 0.1 m. Another fundamental aspect of the engineering geological characterization of the soil coverings involved in landslides was the estimation of the saturated hydraulic conductivity (K_{sat} field) by means of borehole infiltration tests carried out with the Amoozegar permeameter (Amoozegar, 1989), also known as CCHP (Compact Constant Head Parameter) (Reynolds and Elrick, 1986). It allows a constant hydraulic head (H) to be maintained in a borehole (with radius r) under a given influx water discharge (Q), i.e. with a water level lower than the ground surface. This condition is achieved by neutralizing the natural hydraulic head by means of a hydraulic circuit in which the air can entry after overcoming an equivalent pressure (principle of the Mariotte's bottle). This infiltration test is prolonged over a relatively long period of time to minimize effects of the unsaturated flow transitory. The K_{sat} field can be estimated by means of the Glover formula (Zangar, 1953), which is derived from the solution of Darcy's law for a flow through a cylindrical surface, applied in saturated and steady-state conditions (Horton, 1933; Philip, 1957):

$$Ksat_{field} = \frac{C \times Q}{2 \times \pi \times H^2}$$
$$where: \; C = \sinh^{1}\left(H/r\right)\left[\left(r/H\right)^{2} + 1\right]^{1/2} + r/H \tag{2}$$

In a test pit representative of the stratigraphic condition (T4 in Fig. 2), three series of 9 undisturbed soil samples were taken for each soil horizon investigated, respectively at 0.50 m, 1.50 m and 2.50 m of depth, during the same period as the geotechnical and geophysical field testing. Specifically, the soil samples were collected by gently pushing

plastic tube samplers (diameter of 80 mm and length of 150 mm) vertically into the soil after digging to the desired depth and forming a horizontal surface (see photograph in Fig. 10 for an example of sampling). For each series, 2 or 3 soil samples were characterized by geotechnical laboratory methods, while the others were used for the characterization of geophysical properties. The soil samples were tested in laboratory for the characterization of both the physical and index properties, needed for the classification with the USCS international system (ASTM D2487-06, 2006), and the geophysical properties.

3.1.2. Geotechnical laboratory testing

Geotechnical index properties were determined using standard laboratory procedures: particle specific gravity (*Gs*), grain size analysis by both sieving and sedimentation methods, Atterberg limits (w_L and w_P) and Plasticity Index ($PI = w_L - w_P$); Soil Organic Matter (SOM). Porosity (*n*) and void ratio (*e*) were also estimated. The laboratory tests were carried out according to the ASTM and BS standards for the grain size (ASTM D421; ASTM D2217; ASTM D422), consistency limits assessment (ASTM D4318; British Standard 1377) and loss on ignition technique (ASTM D 2974).

Relationships between volumetric water content (θ) and soil water pressure head (*h*) were estimated using empirical pedotransfer functions (Saxton and Rawls, 2006; Saxton and Willey, 2006) based on gravel content and relative content of sand, silt and clay grain size fractions as well as organic matter content and porosity. Soil Water Retention Curves (SWRCs) were then estimated by interpolation of θ and *h* data by means of the van Genuchten model (1980):

$$\theta_e = \frac{\theta_h - \theta_r}{\theta_s - \theta_r} = \frac{1}{(1 + \alpha[h]^n)^m}, \quad (3)$$

where: θ_e is the effective saturation [dimensionless]; θ_h [$cm^3 \cdot cm^{-3}$] is the volumetric water content corresponding to each value of soil water pressure head *h* [cm] and saturation degree; θ_s and θ_r [$cm^3 \cdot cm^{-3}$] are the saturated and residual water contents, respectively; α[cm^{-1}], *n* [dimensionless] and m = 1–1/n [dimensionless] are the fitting parameters of the van Genuchten equation, which were obtained using the RETC software (van Genuchten et al., 1994) by minimizing the standard deviation between experimental data and model.

3.2. Geophysical study

3.2.1. Geophysical field testing

Numerous examples in the literature clearly demonstrate the wide applicability of geophysical investigations for the study of potential landslide hazard areas, both in terms of measurement techniques and geological settings (e.g. Jongmans and Garambois, 2007). The main information that these methods can provide are the identification of the vertical and lateral limits of the landslide body (i.e. differentiation between soil covering and bedrock) and the characterization of the layers (horizons) that form the soil covering. However, it should be emphasized that electrical and electromagnetic methods are also capable of detecting and characterizing the occurrence of groundwater or soil moisture within the investigated underground volume, due to the close correlation between the electrical parameters provided by these methods and the water content permeating the investigated buried geological formations. Given the purpose of the present study, two electrical methods, i.e. electrical resistivity tomography (ERT) and self-potential (SP), were chosen to define the electro-stratigraphy of the soil covering and the physical conditions of both the soil horizons and the underlying bedrock. It should be noted that while ERT prospecting in 2D or 3D mode is one of the most widely used electrical geophysical techniques for landslide hazard assessment (e.g. Di Maio and Piegari, 2011; Perrone et al., 2014; Gance et al., 2016; Di Maio et al., 2020; Zhang et al., 2021), SP surveys, when combined with ERT techniques, have been proven to be particularly useful for the study of the groundwater flow (e.g. Thirard et al., 2020 and references therein). However, to the best of our knowledge, there are no examples of the application of the SP method to the study of shallow landslides involving the ash-fall pyroclastic soils mantling the slopes of the *peri*-volcanic mountain areas of the Campania region (southern Italy).

3.2.1.1. ERT survey. The ERT prospection consists of obtaining the distribution of apparent electrical resistivity values in the vertical cross-section along a survey profile (2D mode) or in a volume (3D mode) by placing a 3D electrode layout on the ground surface (e.g. Loke and Barker, 1996a). The distribution of the real resistivity values is then obtained by inverting the estimated apparent resistivity data through 2D or 3D inversion procedures, usually based on linearized least-square methods with local optimization techniques (e.g. Loke and Barker, 1996b; Loke and Dahlin, 2002; Papadopoulos et al., 2010). If it is not possible to arrange a 3D electrode array, it is common practice to merge the results of a number of 2D ERTs along parallel profiles and to invert the acquired apparent resistivity data using 3D inversion approaches (pseudo-3D mode) (e.g. Dahlin and Loke, 1997).

The ERT survey in the study area consisted of 2D tomographies carried out along 11 parallel profiles, 47 m long and 2 m apart, located on a slope with little rough morphology (yellow rectangle in Fig. 2), but with an elevation difference of about 14 m between the first and the last profile (Fig. 3a). Apparent resistivity data were acquired by the IRIS-SYSCAL PRO georesistivimeter, equipped with multi-electrode cables characterized by an inter-electrode spacing of 1 m (Fig. 3b, c). The pole-dipole electrode configuration was used, which allowed an investigation depth of about 15 m below ground level (b.g.l.). After filtering the collected data to remove any signals due to noise, the RES2DINV software (Loke and Barker, 1996b; Loke, 2004) was used to invert the apparent resistivity values observed along each measurement profile, taking into account the true topography of the profiles ranging from approximately 349 to 353 m a.s.l.. Due to the high-spatial resolution of the 2D ERT survey, the acquired data were also inverted using a pseudo-3D inversion scheme implemented by the RES3DINV algorithm. For both the 2D and 3D inversions, the finite-element method and the complete Gauss-Newton inversion algorithm were chosen to relate the model parameters to the model response and to determine the change in the model parameters (Loke and Barker, 1996b; Loke and Dahlin, 2002), respectively. The root mean square (RMS) error was found to be less than 3 % and 4 % for the 2D and 3D inversions, respectively, reflecting the high reliability of the obtained resistivity models, which are shown in Figs. 6 and 7.

3.2.1.2. SP survey. SP prospection consists in the measurement of natural electrical potential difference (ddp) on the ground surface due to anomalous electrical charge distributions in the subsoil. They can be generated by different phenomena, such as redox reactions around ore/metallic bodies, electrochemical processes related to zones with different ionic concentrations and electrokinetic phenomena associated with underground fluid and/or heat flow circulation (e.g. Revil and Jardani, 2013 and references therein). In hydrogeological problems, the electrokinetic mechanisms are mainly responsible for the SP anomalies observed at the ground surface (e.g. Revil et al., 2003; Soueid Ahmed et al., 2016).

The SP survey on the Ischia Island was carried out along the ERT profiles shown in Fig. 3a. To obtain a network of intercorrelated measurements, the natural ddp values were continuously collected between pairs of adjacent points, 1 m apart, belonging to the whole circuit formed by the 11 ERTs (Figs. 2 and 3a). This acquisition mode allows the application of reference and closure corrections to reduce cumulative errors due, for example, to cultural noise (Barde-Cabusson et al., 2021 and references therein). A high-impedance voltmeter (sensitivity 0.1 mV) and two non-polarizable copper electrodes immersed in a copper sulfate solution were used for data acquisition (Fig. 3d). The SP drops

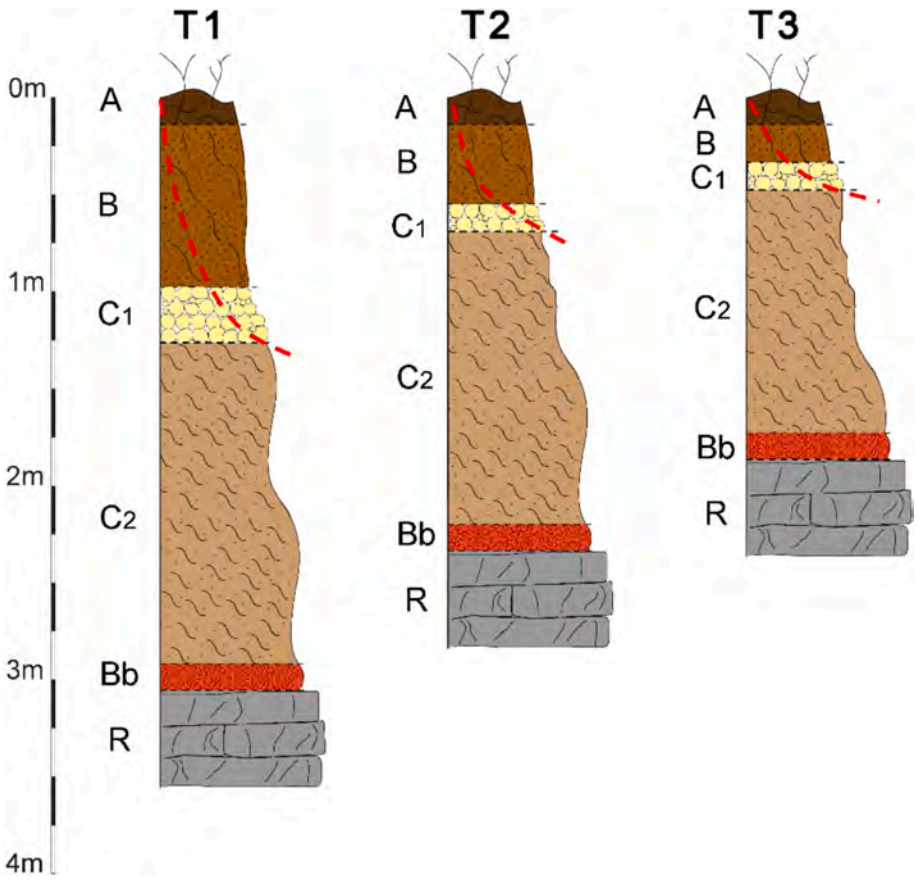

Fig. 4. Stratigraphic columns reconstructed at the tops of landslides main scarps (cfr. Fig. 2). The stratigraphic characterization is based on the nomenclature of the main pedologic soil horizons (Soil Science Division Staff, 2017; USDA, 2022). The red dashed lines indicate the trace of the sliding surface which were inferred based on stratigraphic observations and topographic measurements carried out along the landslide main scarp and flanks. The depths are true (stratigraphic thickness), i.e. calculated perpendicularly to the slope surface.

along the circuit were recorded between two consecutive measuring points when the signal reached a steady state.

To get information on the depth location of the polarization field sources, the collected SP data were processed using a 3D tomographic inversion method that considers the topographic effects on the acquired data (Patella, 1997; Di Maio et al., 1998; 2000). Basically, the method consists of evaluating the cross-correlation function between the observed electric field and the field expected from a synthetic electric source located at any point of the investigated subsurface volume. Through an appropriate normalization process of the cross-correlation function (Patella et al., 1997), a Charge Occurrence Function (COF) is obtained, which is constrained to vary between −1 and 1, with maximum negative and positive values indicating a major occurrence of negative and positive charge accumulation zones, respectively.

3.2.2. Geophysical laboratory testing: Resistivity versus saturation degree curves

To reconstruct a physical model of the landslide source areas at the slope scale, considering also the spatial distribution of the saturation degree (θ_e), laboratory resistivity (ρ) measurements were carried out at varying values of volumetric soil water content (θ) on samples collected from the investigated ash-fall pyroclastic soil cover (see Section 3.1.1). Specifically, a total of 11 samples representative of three different pyroclastic soil horizons, taken at depths of 0.50 m (5 samples), 1.50 m (3 samples) and 2.50 m (3 samples), were analyzed. To simulate in-situ conditions, the resistivity measurements were performed at room temperature and standard pressure on samples saturated with rainwater, characterized by an electrical conductivity of 152 μS/cm, using the Wenner four-electrode technique (e.g. Taylor and Barker, 2002). The resistivity vs. saturation degree curves for the analyzed samples were obtained by oven drying them and evaluating the effective saturation values, θ_e, (for details of the experimental approach, the reader is referred to Di Maio and Piegari (2011) and De Vita et al. (2012).

4. Results

The coupled geotechnical and geophysical characterizations, both based on field and laboratory measurements and tests, allowed the reconstruction of respective conceptual and physical models that resemble the features of the landslide source areas. The two models were successively integrated with each other to enhance the understanding of factors favoring the landslide susceptibility, as well as the hydrological conditions preparing and leading to the landslide triggering. The results of the respective characterizations are reported below.

4.1. Field characterizations of landslide source areas

4.1.1. Engineering geological model

The test pits dug in the landslide source areas, at the tops of landslides crowns (Fig. 2), allowed the identification of a common stratigraphic setting. Taking into account the lithological identification of soils and the nomenclature of the principal pedologic soil horizons (Soil Science Division Staff, 2017; USDA, 2022) and USCS classification (ASTM D2487-06, 2006), the following series of ash-fall pyroclastic soils was recognized in all the cases (Fig. 4): 1) A soil horizon, classifiable as organic soil (Pt); 2) B soil horizon, mainly characterized by weathered pumiceous pyroclasts with grain size ranging from lapilli to coarse ash, dispersed in a slightly organic sandy-silt matrix, classifiable as sand with

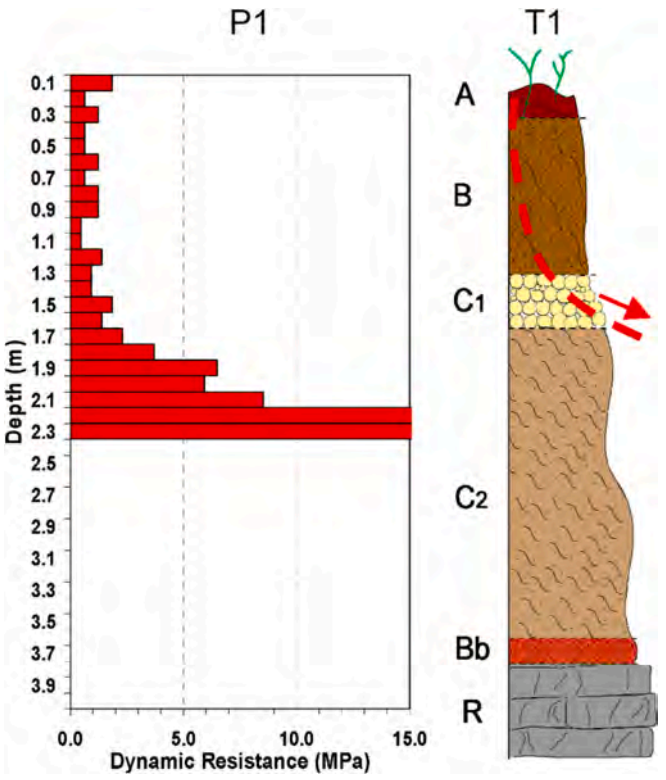

Fig. 5. Example of comparison between the dynamic penetrometer log executed for the landslide 2, expressed in terms of dynamic resistance (Rd), and the stratigraphic column reconstructed at the landslide top (TP1 in Fig. 2). The red dashed line indicates the trace of the sliding surface.

silt with diffuse root apparatuses and bioturbation structures (SM); 3) upper C horizon (C1), consisting of pumiceous and subordinately scoriaceous pyroclasts with low weathering degree, locally reworked, with grain size ranging from lapilli to coarse ash (with maximum dimension up to 20 mm), classifiable as gravel and sand with silt (GM); 4) lower C horizon (C2), made of light brown compact ash with sporadic presence of reddish crusts, classifiable as low plasticity silt (SM); 5) Bb horizon, defined as a buried B layer, therefore assimilable to a paleosol (SM); 6) R horizon, representing the volcanic bedrock, which in the initiation areas is formed of welded scoria in very thick strata with an upstream dipping attitude. The root apparatuses of the vegetation, comprising mainly of chestnut trees, were found to extend down to the B horizon, being scarcer in the deeper soil horizons. From a lithostratigraphic point of view, the volcaniclastic series can be referred to the "Piano Liguori" Formation (Vezzoli, 1988; Orsi et al., 1996), based on the characters of the C soil horizon, which represents the parent material. Regarding the initiation areas, the instability mainly involved the first three soil horizons and only marginally the lower compact ash horizon.

The results of the dynamic penetrometric tests were expressed in terms of dynamic penetration resistance (Rd). The sum of the shallow soil horizons, A + B + C1, results roughly homogeneous in terms of Rd and generally characterized by lower values (average 1.8 MPa), corresponding to a very loose relative density degree. In contrast, the C2 soil horizon, corresponding to the compact ash, is distinguished by higher values of Rd (average 5.3 MPa) (Fig. 5). Owing to the lack of specific empirical correlations, the estimated values of Rd can give qualitative indications about the shear strength values of the tested soils, which can be considered lower in the shallower soil horizons (A, B and C1) compared to the deeper ash soil horizon (C2).

Regarding the estimation of the hydraulic conductivity, the constant head borehole permeability tests showed a saturated field hydraulic conductivity ($K_{sat\ field}$) value of about 1×10^{-4} m·s^{-1} for the B soil horizon, with a very rapid and negligible transient from unsaturated to saturated flow, consistent with the coarse grain size and the low relative density of this soil horizon. In contrast, the test showed a K_{sat} field value of about 1×10^{-7} m·s^{-1} for the lower C2 compact ash horizon. Although the A and C1 soil horizons were not tested due to their small thickness, the results obtained allowed us to recognize a strong difference in the saturated hydraulic conductivity between shallow and deeper soil horizons of about 3 orders of magnitude.

These results allowed the identification of an engineering geological model of the landslide source areas, which is characterized by the proneness of the shallow A, B and C1 soil horizons to slope instability under heavy rainfalls and preceding unfavorable soil hydrological conditions. This conceptual model is supported by the field observations in the landslide source areas, which show the involvement of the shallow soil horizons in landsliding, and by the lower shear strength and high hydraulic conductivity of these soil horizons, which are in contrast with the higher shear strength and lower K_{sat} of the deeper soil horizon not involved in landsliding.

At the same time, as it will be shown in the next sections, this conceptual model supports the validity of the geophysical investigations carried out at a site close to the landslide source areas, characterized by the same soil horizons, as well as the results of geotechnical and geophysical laboratory tests carried out on undisturbed soil samples.

4.1.2. *Geophysical model*

Fig. 6 shows the 2D inversion results obtained for the eleven ERTs carried out along the profiles 2 m apart in the yellow rectangle of Fig. 2. Looking at Fig. 6, it is well evident in all the 2D images the presence of a shallow layer, about 2–3 m thick, characterized by relatively high resistivity (ρ) values ranging from 500 Ωm to 1500 Ωm, with local maxima reaching values of about 3000–4000 Ωm. This layer overlaps a much more conductive soil horizon, about 10 m thick, recognized by ρ values varying from about 40 Ωm to 160 Ωm, with scattered nuclei even more conductive (ρ ~ 20–30 Ωm). Both electro-layers dip to the north and are therefore characterized by a geometry parallel to the slope. At a depth of about 13–14 m from the ground level, the resistivity increases and reaches the highest values observed, i.e. about 7000–8000 Ωm. Referring to the whole sequence of 2D resistivity tomographies (Fig. 6), or, equivalently, to the 3D model in Fig. 7, it can be recognized that the third electro-layer dips to the N at a greater angle than the first two layers, gradually deepening until it is no longer visible within the investigated subsurface volume.

Fig. 8 shows the SP map of the investigated area. The observed low- and high-frequency SP anomalies can be attributed to electrokinetic causes, as other phenomena, such as electrochemical and/or mineralization, would be unlikely for the geological materials present in the study area. Therefore, it is plausible to assume that the water regime of the slope under investigation is responsible for the electrical charge accumulations induced along discontinuities separating media with different electrical properties. Specifically, relatively deep sources due to different lithological/stratigraphic characteristics of the ash-fall pyroclastic soil horizons would be responsible for the relatively low-frequency anomalies observed in the northern and southern sectors of the study area. Conversely, the higher frequency anomalies observed in the central sector of the area may be related to shallower local sources. In other words, the SP map (Fig. 8) highlights the occurrence of a relatively deep dipolar field, oriented approximately SW-NE, ascribable to stratigraphic discontinuities, whose trend is locally disrupted by higher frequency anomalies, generally negative, due to rather superficial inhomogeneities of limited extent associated with areas of higher anion concentrations because of the infiltration of gravitational capillary water into the subsoil.

Fig. 9 shows the results of the 3D tomographic inversion of the SP data, which provides the underground electrical charge distributions likely to be responsible for the SP anomalies observed at the surface (see

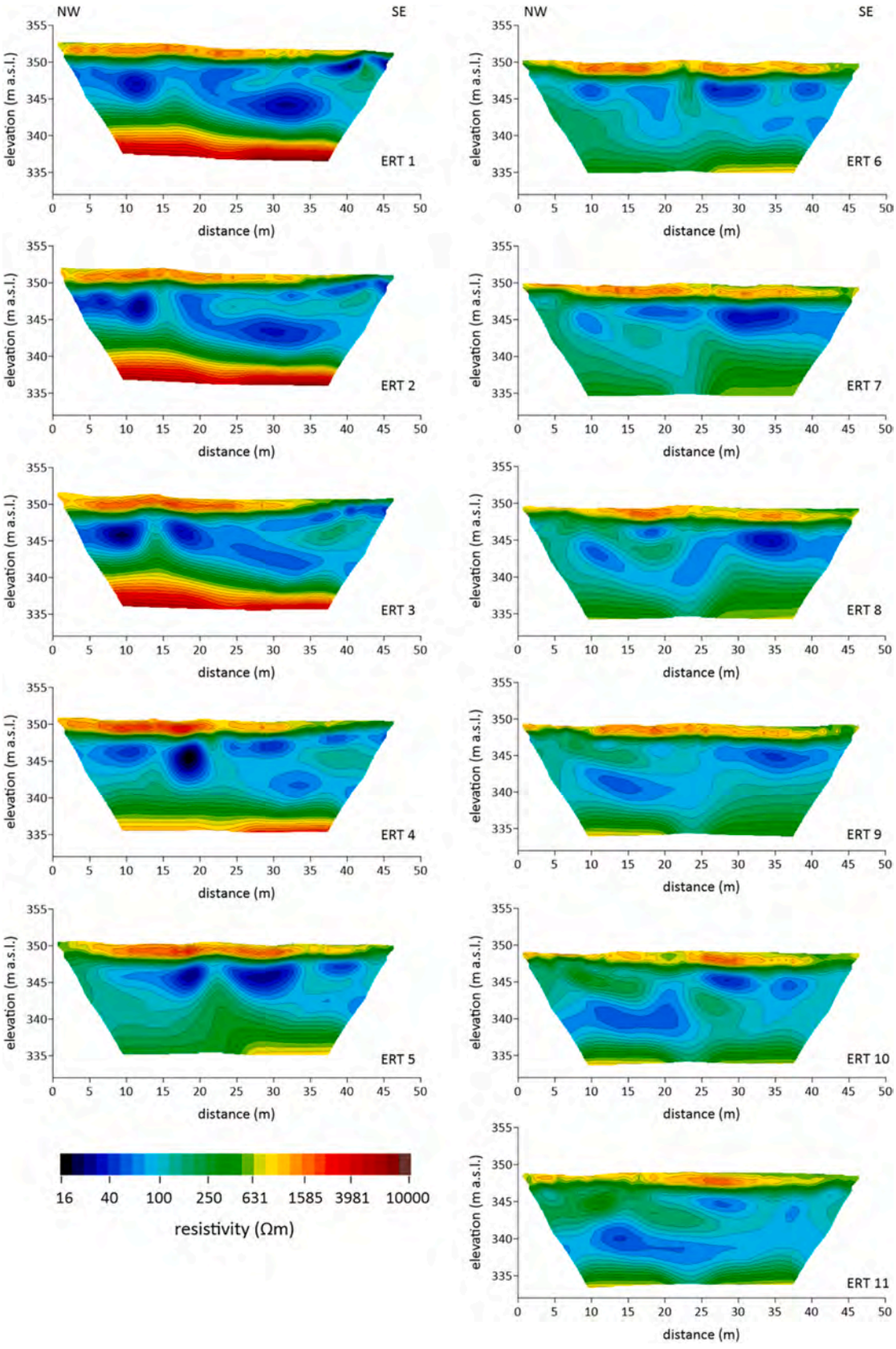

Fig. 6. 2D inversion result of the 2D ERT data acquired along the 11 profiles (yellow box in Figs. 2; Figs. 3a and 3b).

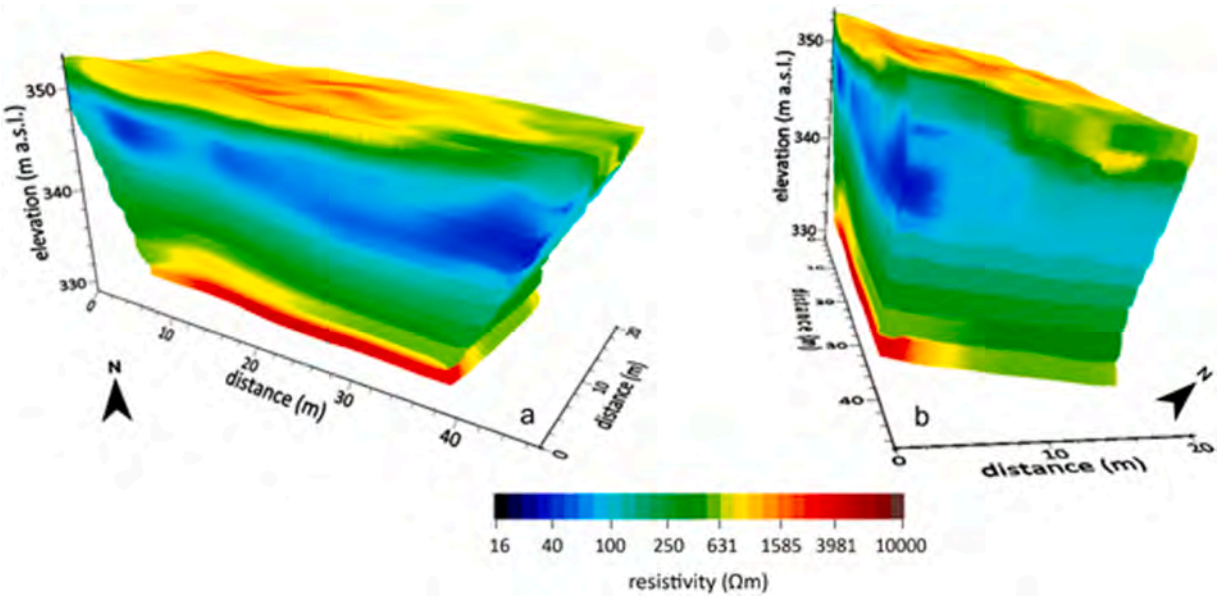

Fig. 7. 3D inversion result of the 2D ERT data acquired along the 11 (yellow box in Figs. 2; Figs. 3a and 3b): a) shown in the north direction; b) in the west direction.

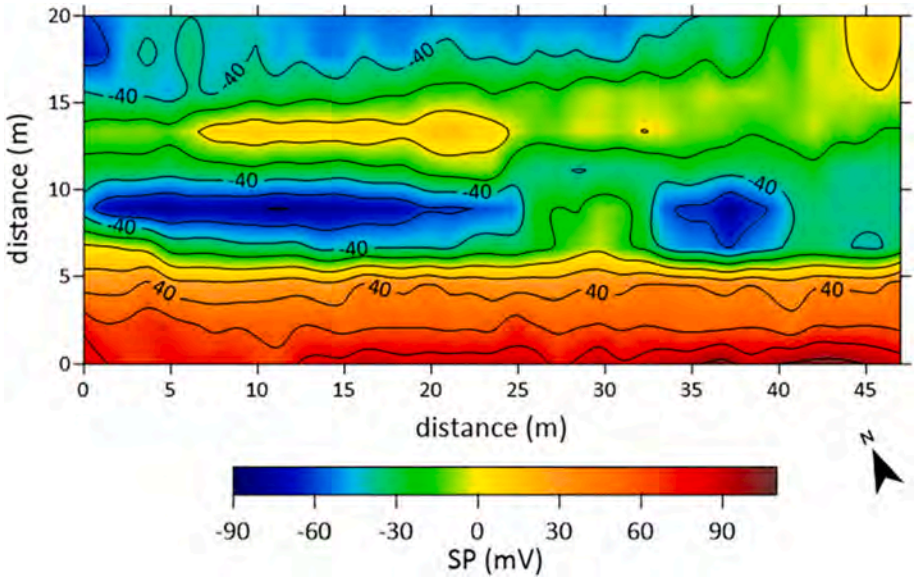

Fig. 8. SP map of the investigated area (yellow box in Figs. 2; Figs. 3a and 3b).

Fig. 8 and Section 3.2.1.2). As can be seen, the computed values of the Charge Occurrence Function (COF) were estimated to be in the range of approximately −0.3 to 0.15.

The most striking correlation between the 3D ERT and SP tomographic images in Figs. 7 and 9, respectively, is the pattern of positive and negative charge accumulations, which roughly resembles the observed resistivity discontinuities. We note that such a pattern (see Fig. 9b), probably due to polarization charges induced along structural and/or physical discontinuities, correspond well to the morphology of the horizontal discontinuity between the first two resistivity layers and to a vertical pattern possibly related to a fracture system characterized by a pronounced fluid mass flow. The latter would thus be responsible for the primary charge sources accountable for the observed positive and negative clusters. Interestingly, the location and depth of the two positive charge accumulations in Fig. 9b correspond to the most conductive parts of the second electro-layer identified in Fig. 7a and 7b with the two dark blue zones. The observed charge configuration can be explained by considering the electro-kinetic origin of the recorded potentials, i.e. streaming potentials (Sharma, 1977). In particular, the positive SP source zones would be associated with groundwater accumulation areas, whereas the negative SP source concentration zones are probably due to water infiltration along the hypothesized fracture system.

4.2. Laboratory geotechnical and geophysical characterizations of landslide materials

Laboratory geotechnical and geophysical characterizations of the soil horizons involved in landsliding were performed on soil samples collected in a test pit dug in the area where the ERT and SP surveys were carried out. Due to operating constraints, this area was identified in the nearby of the landslide source areas (Fig. 2) and considered equivalent for the stratigraphic setting.

The test pit T4 (Figs. 2 and 10), dug by hand tools down to the depth of 2.50 m, revealed a stratigraphic setting formed from the top: A soil

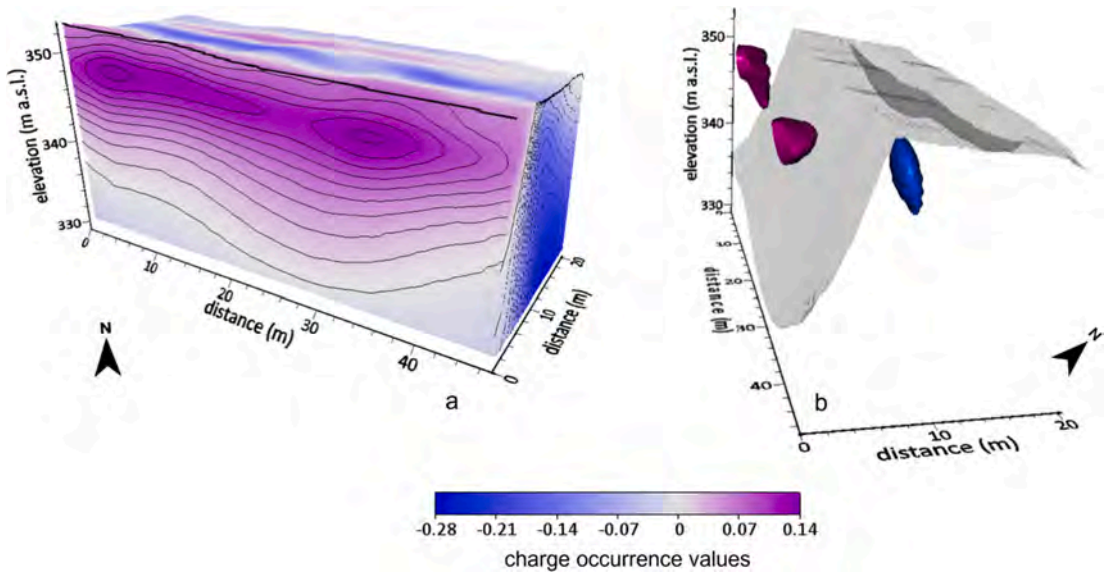

Fig. 9. 3D inversion result of the SP data acquired at Mt. Vezzi (yellow box in Figs. 2; Figs. 3a and 3b)., shown in the north (a) and in the west directions (b). The image (b) highlights volumes characterized by specific ranges of electric charge occurrence values: max negative values (blue shades), max positive values (violet shades) and zero values (grey shades).

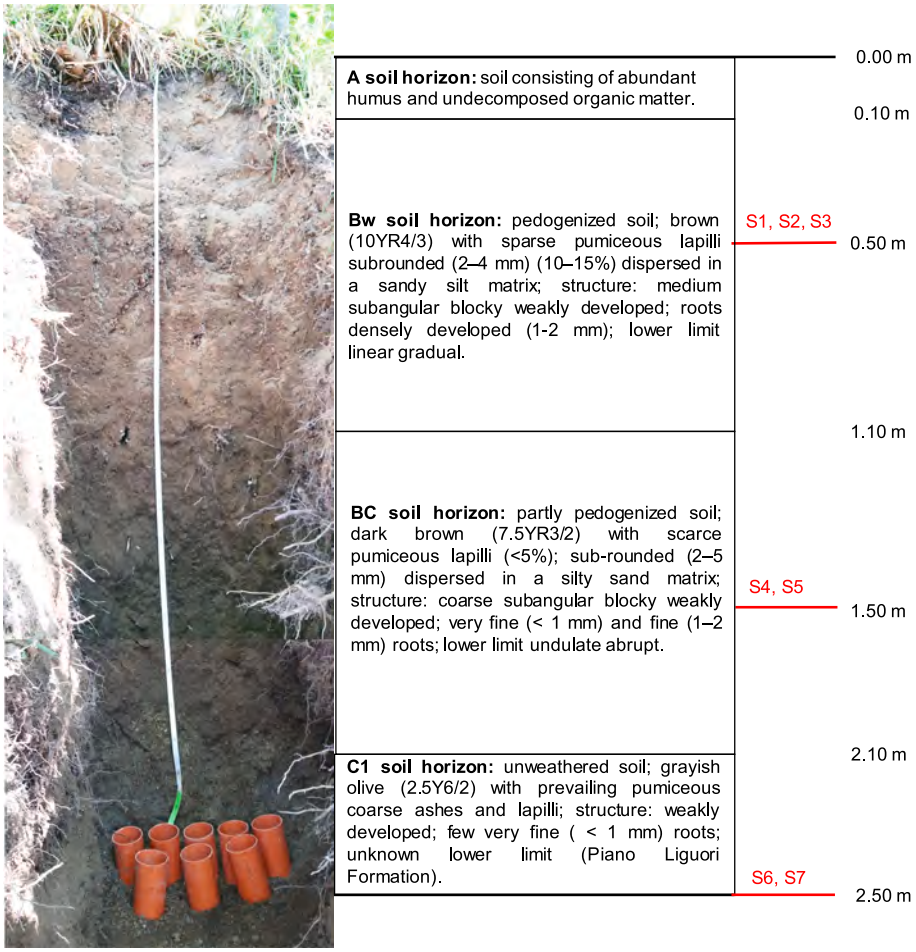

Fig. 10. Photograph of the test pit T4 executed in the area of the ERT and SP surveys (yellow box in Figs. 2; Figs. 3a and 3b) with reconstruction of the local stratigraphy (USDA, 2022) and indication of sampling depths and sample IDs. The plastic cylinder samplers are visible at the bottom of the test pit before being pushed into the soil for the undisturbed sampling.

Table 1
Physical properties of the soil horizons sampled at the Mount di Vezzi, as determined by the geotechnical laboratory tests.

Soil horizon	ID	Bw			BC		C1	
Sample ID	Unit	S1	S2	S3	S4	S5	S6	S7
Depth (m)	m		0.50			1.50		2.50
Dry unit weight (γ_d)	kN·m^3	8.02	8.32	8.31	8.44	9.69	7.36	6.54
Solid particle unit weight (Gs)	kN·m^3	27.65	24.87	25.16	26.18	28.02	25.60	24.86
Porosity (n)	m^3·m^{-3}	0.71	0.67	0.67	0.68	0.65	0.71	0.74
Void ratio (e)	m^3·m^{-3}	2.45	1.99	2.03	2.10	1.89	2.48	2.80

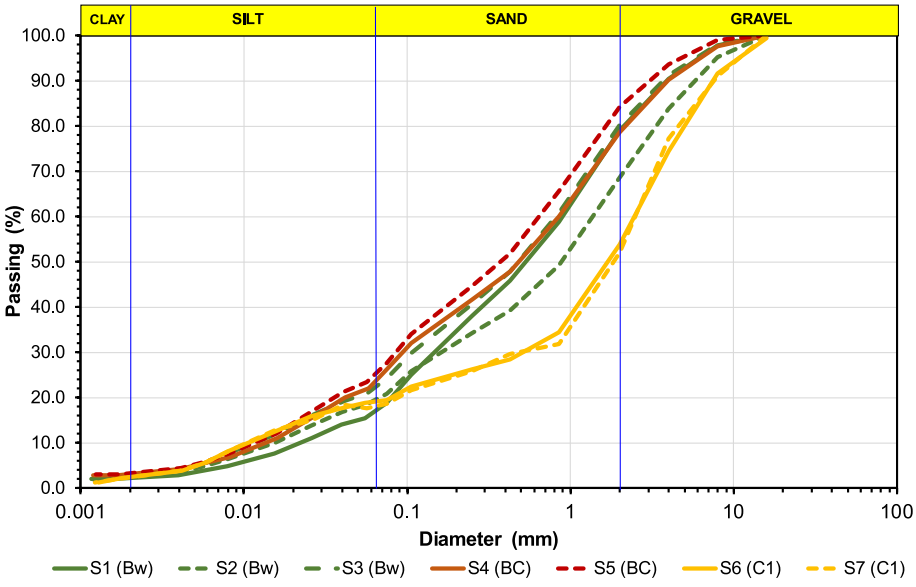

Fig. 11. Grain size curves of soil samples.

horizon, consisting of abundant humus and undecomposed organic matter (0 – 0.10 m depth; true thickness 0.086 m) (Pt); Bw soil horizon, formed by pedogenized soil with pumiceous lapilli dispersed in a sandy silt matrix (0.10 – 1.10 m depth; true thickness 0.86 m) (SM); BC soil horizon, partly pedogenized soil with scarce pumiceous lapilli dispersed in a silty sand matrix (1.10 – 2.10 m depth; true thickness 0.86 m) (SM); C1 soil horizon, formed by unweathered pumiceous lapilli (gravel) and coarse ashes (sand) corresponding to a deposit of the Piano Liguori Formation (2.10 – undefined depth) (GM). Three sets of undisturbed soil samples were collected from the three soil horizons and tested by laboratory geotechnical and geophysical procedures. The deeper C2 soil horizon, found in the landslide source areas, not involved in landsliding due to its higher shear strength and lower permeability, was not intercepted by the test pit.

4.2.1. Geotechnical laboratory characterization

The results of the geotechnical laboratory tests (Table 1) showed values of physical properties consistent with those determined in a previous study for the landslides that occurred on April 30, 2006, at Mount di Vezzi (De Vita et al., 2007) and with those typical of ash-fall pyroclastic soils covering carbonate mountains in the area surrounding the Somma-Vesuvius volcano (De Vita et al., 2013).

The dry unit weight (γ_{dry}) is typically characterized by values lower than that of water, showing a variability with the depth of mean values from 8.21 kN·m^3 of the Bw soil horizon, to 9.06 kN·m^3 of the BC soil horizon to 6.95 kN·m^3 of the C1 soil horizon. The values of the solid particle unit weight (Gs) are fairly constant at around 26.04 kN·m^3. Porosity (n) and void ratio (e) are typically very high compared to other soil types, with respective mean values of 0.68 and 2.15, for the Bw soil horizon, 0.67 and 2.00, for the BC soil horizon and 0.73 and 2.64, for the C1 soil horizon. The lower values of γ_{dry} and the highest values of n and e of the deepest soil horizon are related to its coarser grain size and the intraparticle porosity of pyroclastic soils.

Table 2
Results of the grain size analysis and classification of soil samples according to the USCS system.

Soil horizon	ID	Bw			BC		C1	
Sample ID	Unit	S1	S2	S3	S4	S5	S6	S7
Depth (m)	m		0.50			1.50		2.50
Gravel	%	21.0	31.3	19.8	21.4	15.8	46.2	44.0
Sand	%	62.4	49.5	58.3	55.5	59.5	34.8	38.2
Silt	%	14.5	16.8	19.3	20.2	21.7	16.7	15.5
Clay	%	2.1	2.4	2.7	2.9	3.1	2.3	2.3
Soil organic matter	%	7.2	6.5	6.8	3.9	3.5	1.2	1.0
USCS	–	SM	SM	SM	SM	SM	GM	GM

Index properties, grain size and Atterberg's limits were also determined on the soil samples, allowing their classification according to the USCS system (Fig. 11; Table 2). The mean values of gravel, sand, silt and clay grain size classes were estimated for each soil horizon, respectively as: 24.0 %, 56.7 %, 16.9 % and 2.4 % for the Bw soil horizon; 18.6 %, 57.5 %, 20.9 %, 3.0 % for the BC soil horizon; 45.1 %, 36.5 %, 16.1 % and 2.3 % for the C1 soil horizon. The results of the grain size analysis confirmed the field observation of the coarser texture of the deepest soil horizons, corresponding to unweathered deposits of the Piano Liguori Formation. According to the USCS system and due to the passing fraction at the ASTM No. 200 sieve (0.075 mm), which is always greater than 12 %, Atterberg's limits were determined on the passing fraction allowing the classification by the Casagrande's plasticity chart (Fig. 12). The results show values of liquid limit (w_L) lower than 50 % and Plasticity

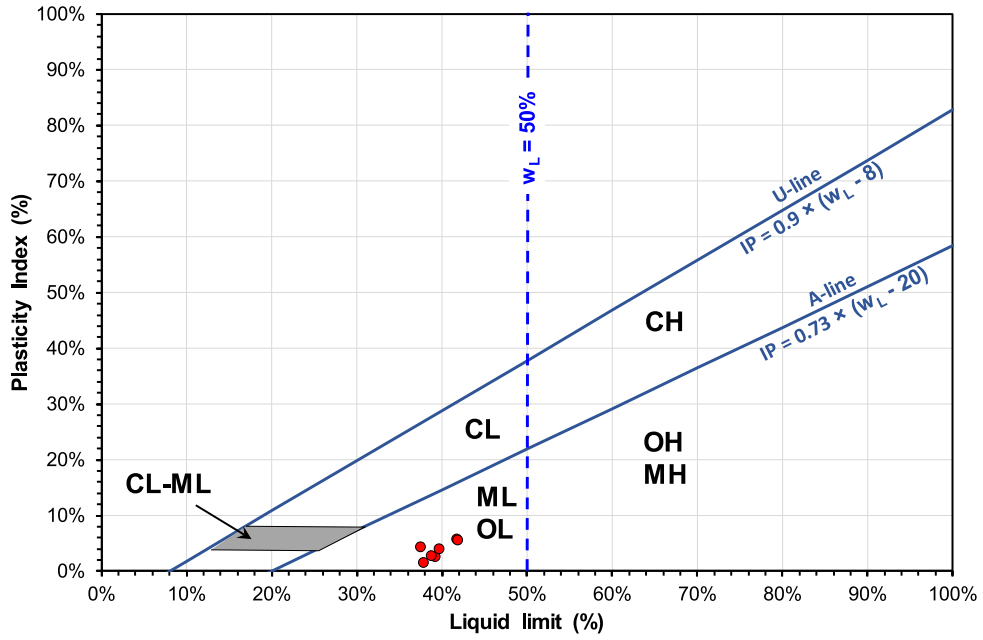

Fig. 12. Results of Atterberg's limits and classification of soil samples by the Casagrande's plasticity chart (USCS classification; ASTM D 2487-83, 1985).

Table 3
Parameters of the van Genuchten model provided by the optimized procedure performed by RETC software of the θ_h and h data obtained by the Saxton pedotransfer functions (Saxton and Rawls, 2006).

Soil horizon	ID	Bw				BC			C1		
Sample ID	Unit	S1	S2	S3	*Mean*	S4	S5	*Mean*	S6	S7	*Mean*
Depth	m	0.50				1.50			2.50		
θ_r	$cm^3 \cdot cm^{-3}$	0.1138	0.1110	0.1099	*0.1116*	0.0084	0.0051	*0.0068*	0.0032	0.0041	*0.0036*
θ_s	$cm^3 \cdot cm^{-3}$	0.5876	0.5857	0.5921	*0.5885*	0.4989	0.5379	*0.5184*	0.4625	0.4603	*0.4614*
α	cm^{-1}	0.0060	0.0062	0.0063	*0.0062*	0.0058	0.0082	*0.0070*	0.0068	0.0070	*0.0069*
n	–	2.8496	2.5807	2.5707	*2.667*	2.8246	1.8378	*2.3312*	2.0142	1.9558	*1.985*

Index (PI) lower than 10 %, which allow the classification of the passing fraction as low plasticity silt (ML). Considering these results, the soil samples can be classified as sand with silt (SM) according to the USCS system.

Based on the results of the grain size and soil organic matter analyses (Table 2), pedotransfer functions (Saxton and Rawls, 2006) were applied to estimate the coupled value of volumetric water content (θ) and soil water pressure head (*h*), from which SWRCs were reconstructed and optimized parameters of the van Genucthen model were obtained by the RETC software (Table 3).

4.2.2. *Geophysical laboratory characterization*

Experimental data of effective saturation (θ_e) vs. electrical resistivity (ρ) of the 3 sets of undisturbed soil samples collected from the selected sampling depths (Fig. 10) were obtained by geophysical laboratory tests (Fig. 13), allowing the reconstruction of empirical power-law functions (Table 4). A simple power-law, corresponding to the well-known Archie's relationship (Archie, 1942), was obtained only for the curves related to the soil samples of the shallow soil horizon (Bw), while the fitting curves of the samples belonging to the other two deeper soil horizons (BC and C1 soil horizon) required slightly modified fit functions:

$$\theta_e = \left(\frac{\rho}{a}\right)^{\frac{1}{b}} \tag{4}$$

$$\theta_e = \left(\frac{\rho}{a}\right)^{\frac{1}{b}} - 1 \tag{5}$$

where *a* is the resistivity of the fully water-saturated rock sample and *m* is the cementation exponent (Glover, 2016). It is interesting to note that the value of *a* in Table 4, which constrains the resistivity value of each investigated soil horizon at zero saturation (i.e. $\theta_e = 0$), gives a resistivity estimate for the deepest horizon that is greater than those characterizing the first two soil horizons. This is in good agreement with the lithological nature of the C1 soil horizon, which is formed by coarser soils (see par. 4.2.1).

By extracting the soil water pressure head (*h*) from eq. (3),

$$h = \frac{\left[\left(\frac{1}{\theta_e}\right)^{\frac{1}{m}} - 1\right]^{\frac{1}{n}}}{\alpha}, \tag{6}$$

and combining it with the eqs. (4) and (5), the following empirical equations relating soil water pressure head to soil resistivity were reconstructed [eqs. (7) and (8)]:

$$h = \frac{\left[\left(\left(\frac{\rho}{a}\right)^{-\frac{1}{b}}\right)^{\frac{1}{m}} - 1\right]^{\frac{1}{n}}}{\alpha}, \tag{7}$$

$$h = \frac{\left[\left(\left(\frac{\rho}{a}\right)^{-\frac{1}{b}} - 1\right)^{\frac{1}{m}} - 1\right]^{\frac{1}{n}}}{\alpha}. \tag{8}$$

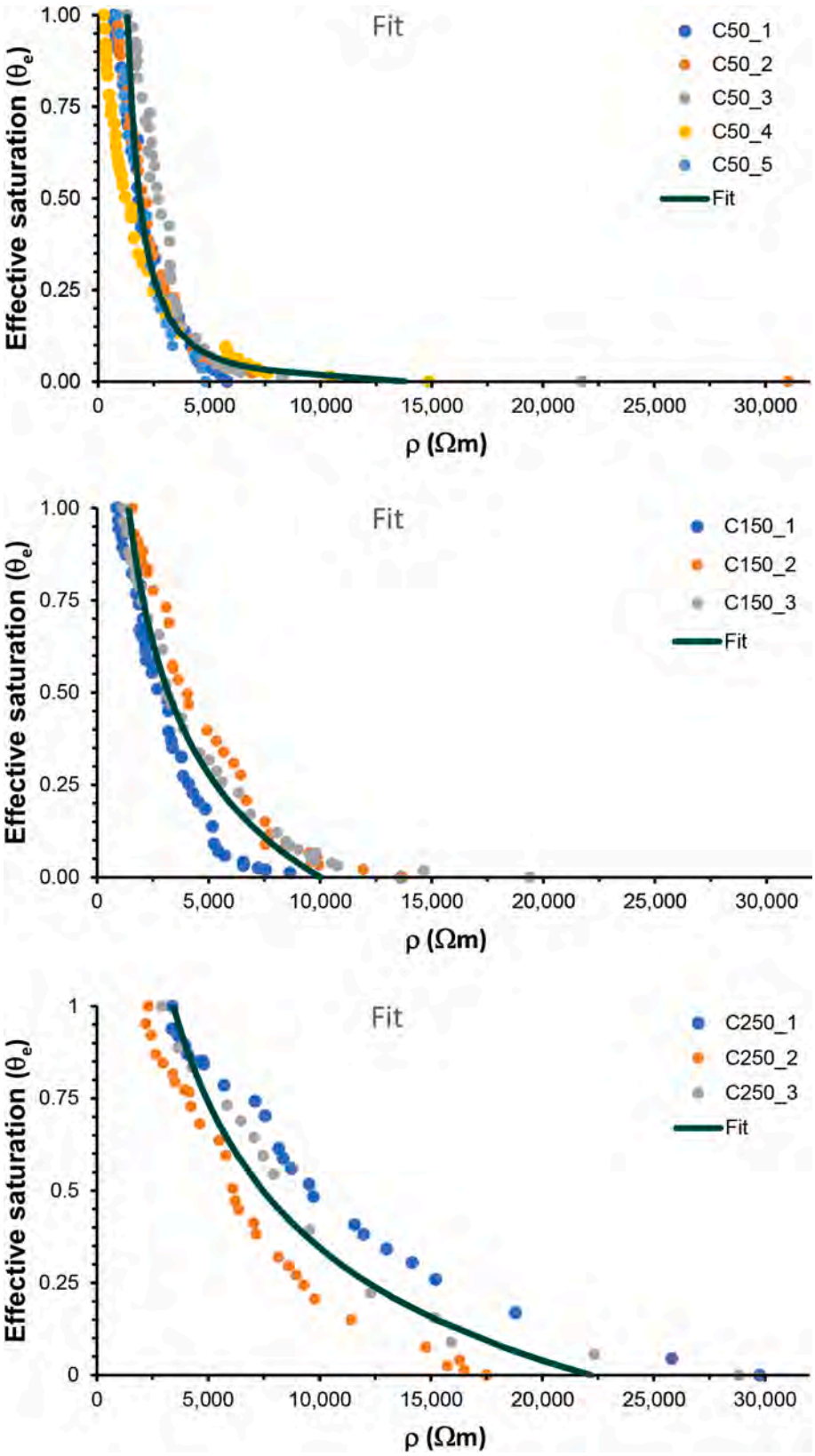

Fig. 13. Effective saturation (θ_e) versus resistivity (ρ) curves (colored dots) for the analyzed samples belonging to the three selected sampling depths: 0.50 m (a), 1.50 m (b) and 2.50 m (c). The dark green solid lines show the fitting curves obtained by the functions given in Table 4.

Table 4
Fitting functions of the experimental curves θ_e vs ρ (Fig. 13) for the different soil horizons analyzed, where *a* is the resistivity of the porous medium for $\theta_e = 0$, the exponent *b* is related to the properties of the medium and R^2 is the coefficient of determination.

Horizon	Depth (m)	Fitting function	a (Ωm)	b	R^2
Bw	0.50	Eq. (4)	1313 ± 45	−0.51 ± 0.01	0.90
BC	1.50	Eq. (5)	10010 ± 551	−2.82 ± 0.28	0.86
C1	2.50	Eq. (5)	22194 ± 888	−2.69 ± 0.17	0.83

Using the optimized fitting parameters of the van Genuchten equation (Table 3) and the relationship linking the soil resistivity (ρ) to the effective saturation (θ_e) (Table 4), empirical equations relating the soil water pressure head (*h*) to the soil resistivity were found (Fig. 14).

5. Discussion

In this work, an attempt of extending field and laboratory characterizations of soil coverings involved in rainfall-induced shallow landslides was made by integrating geotechnical and geophysical techniques.

The proposed approach is to be considered novel because it aims to integrate the site-specific significance of geotechnical investigations, which are based only on local measurements and samplings and are therefore reasonably related to a volume scale varying from 10^{-3} to 10^{-1} m^3, with geoelectrical surveys, which involve underground volumes varying in the range $10^0 - 10^3$ m^3, and thus much more representative of the landslide scale. Furthermore, the results of this work demonstrate that the integration of both methodologies can be functional for two distinct objectives in the field to shallow rainfall-induced landslides hazard assessment.

The first is the reconstruction of the slope physical model, based on the integration of slope engineering geological and geophysical models, incorporating soil horizons prone to landsliding and their spatial features at the landslide scale, as well as geotechnical and geophysical properties. Without this type of integration, the slope physical model needed for modeling slope stability is usually reconstructed by spatial interpolations of stratigraphic and geotechnical data observed at the site-specific scale, which are affected by approximations depending on the distance between investigation points. Instead, our approach, relying on high-resolution 2D/3D images of the subsurface resistivity patterns, not only favor the spatial interpolation of local stratigraphic data obtained from test pits and dynamic penetration tests, but also allows to explore depths that would otherwise require the use of heavy drilling machinery, which is prevented by steep morphology and dense wood vegetation. In this regard, it is important to emphasize that the resistivity models (Fig. 6) are consistent and match well with those obtained from the geotechnical field investigations (Fig. 5). Indeed, they show an upper resistivity horizon (ρ > 250 Ωm) corresponding to the A, B and C_1 soil horizons, an intermediate resistivity horizon (ρ < 250 Ωm) corresponding to the C_2 soil horizon and a deeper resistivity horizon (ρ > 250 Ωm) corresponding to the local volcanic bedrock.

The second aspect concerns the assessment of the hydrological status of the soil covering, which is known to be predisposed to rainfall triggering (Fusco et al., 2017; Greco et al., 2023). This is based on the good correlation of the resistivity (ρ) with the soil water content (θ) and soil water pressure head (*h*), as well as on the close relationship between the SP anomaly pattern and the accumulation and movement of groundwater flows associated with landslide reactivation (Sujitapan et al., 2019). In fact, rainfall could exert a major control on the SP given that the streaming potential is likely to be the main SP mechanism in potential debris-flow source areas. These correlations open the application of geoelectrical surveys to soil hydrological monitoring of soil mantled slopes prone to landsliding and to the setting of LEWS, in particular for what regards the antecedent hydrological conditions of the soil coverings. Indeed, the role of the antecedent hydrological status of the soil cover on the rainfall conditions that trigger shallow landslides (Napolitano et al., 2016; Fusco et al., 2021; 2022; Rianna et al., 2023; Levinna et al., 2024) is nowadays considered a fundamental part of LEWS, together with the rainfall nowcasting based on meteorological radar. In this regard, the relevance of the soil hydrological monitoring in the definition of LEWS has been demonstrated by many authors (e.g., Collins and Znidarcic, 2004; Sidle and Ochiai, 2006; Lu and Godt, 2013; Bogaard and Greco, 2016) due to the link between the antecedent soil water content, mostly in unsaturated conditions, and the decrease in soil shear strength, which predisposes to slope failure under a given rainfall event. Conversely, the decrease in antecedent volumetric soil water

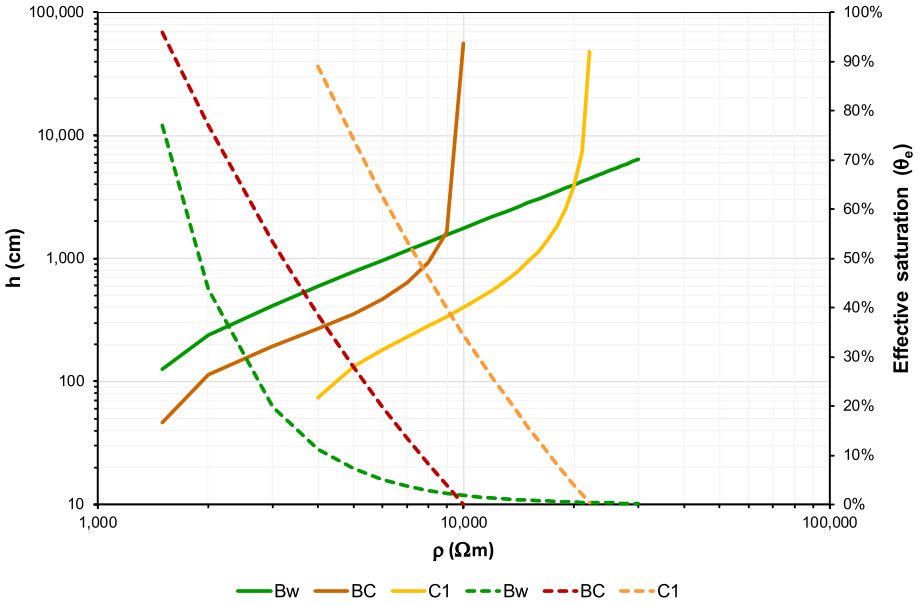

Fig. 14. Continuous lines: relationships between soil resistivity (ρ) and soil water pressure head (*h*) for the three soil horizons considered. Dashed lines: relationships between soil resistivity and effective saturation (θ_e) for the three soil horizons considered.

content reduces the probability of slope instability under the same rainfall condition. Therefore, soil hydrological monitoring has progressively become a fundamental achievement to assess the hydrological response of the slope and to calibrate the hydrological numerical modelling (Greco et al., 2013; Lu and Godt, 2013; Comegna et al., 2016; Fusco et al., 2017; Bordoni et al., 2019; Fusco et al., 2019; 2022). In such a perspective, the application of the relationship between resistivity (ρ) and soil hydrological variables (θ and *h*) can be considered novel because it potentially allows the monitoring of the hydrological status of the soil mantled slopes and the value of the soil water pressure head (*h*), on which both the threshold value of the rainfall triggering shallow landslides (Napolitano et al., 2016; Fusco et al., 2022; Rianna et al., 2023; Levinna et al., 2024) and the variable shear strength under unsaturated conditions (Lu and Likos, 2004) depend. Moreover, our results open new perspectives regarding their potential uses in data-driven or physically based modeling LEWS based on considering the antecedent hydrological status of the soil cover.

Furthermore, continuous SP monitoring could help to identify changes in the distribution of the SP source accumulation zones related to the groundwater flow dynamics (Colangelo et al., 2006). These achievements can be considered as a practical and cost-effective advancement of traditional soil hydrological monitoring techniques, which are based on the use of tensiometers or other sensors (time-domain reflectometer and electrical capacitance meter), whose significance is strictly site-specific and potentially affected by installation problems.

Limitations of the proposed approach include the spatial heterogeneity of hydrological and geotechnical parameters of soil horizons sampled for laboratory tests, which would reduce the reliability of correlations with geophysical properties at larger scales. This in turn may lead to uncertainties in model outputs, i.e. may affect the accuracy of predictions of the spatial and temporal occurrence of landslides. However, it should be noted that previous studies by the authors in similar landslide contexts (Di Maio et al., 2020; Pirone et al., 2023), in favorable homogeneous stratigraphic conditions, have shown good agreement between the volumetric water content obtained by field time domain reflectometry measurements and that estimated by combining ERT measurements with the resistivity vs. water content characteristics curves of different soil horizons. Moreover, although geophysical prospecting methods can define the buried stratigraphic setting and its physical properties over subsurface volumes, they are constrained by lateral and vertical resolution. Particularly for spatially highly heterogeneous soil covers, this constrain could prevent the accurate identification of predisposing factors for very shallow landslide occurrence.

Further developments of the research would require continuous monitoring of the soil hydrological regime of the pyroclastic soil cover, coupled with repeated geoelectrical surveys over time, to assess not only seasonal variability but also the effects of long-term climate change on hydrological factors predisposing to and triggering slope instability (Liu et al., 2024; Ye et al., 2024). Finally, an expected future advancement of the research would be the coupling of resistivity measurements with slope stability analysis through the knowledge of shear strength data.

6. Conclusions

Due to the increasing risk from shallow rainfall-induced landslides, which is favored by both the increased frequency and intensity of rainstorms induced by the climate change and the expansion of urbanized areas in footslope zones, the research into effective methods for assessing the hazard from rainfall-induced shallow landslides is a major scientific challenge. Therefore, the integration of geotechnical and geoelectrical techniques appears to be a promising approach for a better definition of the physical models of potentially unstable slopes, which is needed for the assessment of slope stability. This extended concept of the slope model, which can be named physical model, is intended to contribute to the estimation of the spatial component of the landslide hazard, namely the landslide susceptibility. Moreover, the coupling of geophysical and geotechnical properties, such as resistivity, volumetric water content and soil water pressure head, enables the use of resistivity as a proxy for the hydrological status of the soil mantled slopes. On the other hand, the SP appears to be suitable for monitoring groundwater conditions, thus providing precursory information for early warning of landslides. This allows the use of geoelectrical surveys to estimate the hydrological status of the soil cover at the scale of the initial stage of shallow landslides ($10^0 – 10^2$ m^3), which in turn allows the estimation of the temporal component of the landslide hazard and supports the setting of Landslide Early Warning Systems (LEWS) based on rainfall thresholds.

The approach proposed in this work is meant to be a proof of concept that can be developed into standard procedures and applied in all areas worldwide affected by shallow rainfall-induced landslides hazard.

CRediT authorship contribution statement

R. Di Maio: Writing – review & editing, Writing – original draft, Validation, Supervision, Resources, Project administration, Methodology, Investigation, Funding acquisition, Formal analysis, Data curation, Conceptualization. **R. Salone:** Visualization, Investigation, Formal analysis, Data curation. **C. De Paola:** Visualization, Investigation, Formal analysis, Data curation. **R. Carbonari:** Writing – review & editing, Formal analysis, Data curation. **D. Cusano:** Writing – review & editing, Visualization, Formal analysis, Data curation. **P. De Vita:** Writing – review & editing, Writing – original draft, Validation, Supervision, Resources, Project administration, Methodology, Investigation, Funding acquisition, Formal analysis, Data curation, Conceptualization.

Funding

The research was funded by European Union – NextGenerationEU – Mission 4 "Education and Research" – Component 2 "From Research to Business" – Investment 3.1 "Fund for the realization of an integrated system of research and innovation infrastructures" – Project IR0000037 – GeoSciences IR.

Declaration of competing interest

The authors declare the following financial interests/personal relationships which may be considered as potential competing interests: Pantaleone De Vita reports financial support and article publishing charges were provided by University of Naples Federico II Department of Earth Sciences Environment and Resources. If there are other authors, they declare that they have no known competing financial interests or personal relationships that could have appeared to influence the work reported in this paper.

Acknowledgments

Authors thank the project GeoSciences IR (IR0000037) managed by Istituto Superiore per la Protezione e la Ricerca Ambientale (ISPRA) and funded by European Union. Moreover, Authors thank Dr. Enrico Di Clemente, the technician in chief of the laboratory of Engineering Geology and Hydrogeology of the Department of Earth, Environment and Resources Sciences, for the valuable assistance. The authors are very grateful to the Editor and the two anonymous reviewers for their insightful comments and suggestions, which helped to improve the quality of the manuscript.

Data availability

Data will be made available on request.

References

Alvioli, M., De Matteo, A., Castaldo, R., Tizzani, P., Reichenbach, P., 2022. Three-dimensional simulations of rockfalls in Ischia, Southern Italy, and preliminary susceptibility zonation. Geomat. Nat. Haz. Risk 13 (1), 2712–2736. https://doi.org/10.1080/19475705.2022.2131472.

Amoozegar, A., 1989. A compact constant head permeameter for measuring saturated hydraulic conductivity of the vadose zone. Soil Sci. Soc. Am. J. 53, 1356–1361. https://doi.org/10.2136/sssaj1989.03615995005300050009x.

Archie, G.E., 1942. The electrical resistivity log as an aid in determining some reservoir characteristics. Pet. Trans. Am. Inst. Min. Metall. Pet. Eng. 146, 54–62. https://doi.org/10.2118/942054-G.

Arnone, E., Noto, L.V., Lepore, C., Bras, R.L., 2011. Physically based and distributed approach to analyse rainfall-triggered landslides at watershed scale. Geomorphology 133 (3–4), 121–131. https://doi.org/10.1016/j.geomorph.2011.03.019.

ASTM D2217, 1998. Standard Practice for Wet Preparation of Soil Samples for Particle-Size Analysis and Determination of Soil Constants. Annual Book of ASTM Standards.

ASTM D421-85, 1998. Practice for dry preparation of soil samples for particle-size analysis and determination of soil constant. Annual Book of American Society for Testing and Material Standards, West Conshohocken, USA, pp 8–9.

ASTM D422-63, 1998. Standard test method for particle-size analysis of soils. Annual Book of American Society for Testing and Material Standards, West Conshohocken, USA, pp 10–17.

ASTM D 2487-83, 1985. Classification of Soils for Engineering Purposes: Annual Book of American Society for Testing and Materials, 4, 395-408.

ASTM D4318, 1984. Standard test method for liquid limit, plastic limit and plasticity index of soil. Annual Books of ASTM Standards.

ASTM-D2974, 2000. Standard Test Methods for Moisture, Ash, and Organic Matter of Peat and Other Organic Soils, ASTM International.

ASTM D 2487-06, 2006. Classification of Soils for Engineering Purposes (Unified Soil Classification System). ASTM International, 100 Barr Harbor Drive, PO Box C700, West Conshohocken, PA 19428-2959, United States.

Baecher, G., Christian, J., 2003. Reliability and Statistics in Geotechnical Engineering. Wiley. ISBN 978-0471498339, 616 p.

Barde-Cabusson, S., Finizola, A., Grobbe, N., 2021. A practical approach for self-potential data acquisition, processing, and visualization. Interpretation 9 (1), T123–T143. https://doi.org/10.1190/int-2020-0012.1.

Baum, R.L., Godt, J.W., 2010. Early warning of rainfall-induced shallow landslides and debris flows in the USA. Landslides 7, 259–272. https://doi.org/10.1007/s10346-009-0177-0.

Beck, H.E., Zimmermann, N.E., McVicar, T.R., Vergopolan, N., Berg, A., Wood, E.F., 2018. Present and future Koppen-Geiger climate classification maps at 1-km resolution. Sci. Data 5, 180214. https://doi.org/10.1038/sdata.2018.214.

Bogaard, T., Greco, R., 2016. Landslide hydrology: from hydrology to pore pressure. WIREs Water 3, 439–459. https://doi.org/10.1002/wat2.1126.

Bordiga, O., 1914. Il nubifragio del 24 ottobre 1910 ne' suoi effetti sulle colture dell'Isola d'Ischia e della costiera amalfitana e le stime dei danni relativi. Atti R. Istituto d'Incoraggiamento, VI, Napoli.

Bordoni, M., Corradini, B., Lucchelli, L., Valentino, R., Bittelli, M., Vivaldi, V., Meisina, C., 2019. Empirical and physically based thresholds for the occurrence of shallow landslides in a prone area of northern Italian Apennines. Water 11 (12), 2653. https://doi.org/10.3390/w11122653.

Borga, M., Dalla Fontana, G., De Ros, D., Marchi, L., 1998. Shallow landslide hazard assessment using a physically based model and digital elevation data. Environ. Geol. 35, 81–88.

British Standard (BS) 1377, 1990. Methods of test for Soils for civil engineering purposes. ISBN 0580176924, 27 p.

Cassan, M., 1988. Les essais in situ en méchanique des sols. Volume 1 réalisation et interpretation. 2ème. ISBN 978-1784051105, 394 p.

CENT/TC 341 N 119 E. 2003. Geotechnical Investigation and Testing – Part 2: Dynamic Probing edition: 146-151. Eyrolles. Paris.

Chen, H.X., Zhang, L.M., 2014. A physically based distributed cell model for predicting regional rainfall-induced shallow slope failures. Eng. Geol. 176, 79–92. https://doi.org/10.1016/j.enggeo.2014.04.011.

Chiesa, S., Civetta, L., De Lucia, M., Orsi, G., Poli, S., 1987. Volcanological evolution of the island of Ischia. Rend. Acc. Sci. Fis. Mat. Napoli. Special Issue 69–83.

Colangelo, G., Lapenna, V., Perrone, A., Piscitelli, S., Telesca, L., 2006. 2D self-potential tomographies for studying groundwater flows in the Varco d'Izzo landslide (Basilicata, southern Italy). Eng. Geol. 88 (3–4), 274–286. https://doi.org/10.1016/j.enggeo.2006.09.014.

Collins, B.D., Znidarcic, D., 2004. Stability analyses of rainfall induced landslides. J. Geotech. Geoenviron. Eng. 130 (4), 362–372. https://doi.org/10.1061/(ASCE)1090-0241(2004)130:4(362).

Comegna, L., Damiano, E., Greco, R., Guida, A., Olivares, L., Picarelli, L., 2016. Field hydrological monitoring of a sloping shallow pyroclastic deposit. Can. Geotech. J. 53 (7), 1125–1137. https://doi.org/10.1139/cgj-2015-0344.

Crawford, M.M., Bryson, L.S., Woolery, E.W., Wang, Z., 2018. Using 2-D electrical resistivity imaging for joint geophysical and geotechnical characterization of shallow landslides. Journal of Applied Geophysics 157, 37–46.

Crawford, M.M., Zhu, J., Webb, S.E., 2015. Geologic, geotechnical, and geophysical investigation of a shallow landslide, eastern Kentucky. Environ. Eng. Geosci. 21 (3), 181–195.

Cruden, D.M., Varnes, D.J., 1996. Landslide types and processes. In: Turner A.K., Schuster R.L. (eds.) Landslides investigation and mitigation. Transportation research board, U.S. National Research Council. Special Report 247, Washington, DC, ISBN 978-1107002067, 3, 36–75.

Dahlin, T., Loke, M.H., 1997. Quasi-3D resistivity imaging: Mapping of 3D structures using two-dimensional DC resistivity techniques. 3rd EEGS Meeting, Mtg., Expanded Abstracts, 143–146, https://doi.org/10.3997/2214-4609.201407298.

de Riso, R., Budetta, P., Calcaterra, D., Santo, A., Del Prete, S., De Luca, C., Di Crescenzo, G., Guarino, P.M., Mele, R., Palma, B., Sgambati, D., 2004. Fenomeni di instabilità dei Monti Lattari e dell'area flegrea (Campania): Scenari di suscettibilità da frana in aree-campione. Quad. Di Geol. Appl. 1 (11), 5–30.

De Vita, P., Di Clemente, E., Rolandi, M., Celico, P., 2007. Engineering geological models of the initial landslides occurred on April 30, 2006, at Mount di Vezzi (Ischia Island, Italy). Italian J. Eng. Geol. Environ. 2, 119–141. https://doi.org/10.4408/IJEGE.2007-02.O-08.

De Vita, P., Di Maio, R., Piegari, E., 2012. A study of the correlation between electrical resistivity and matric suction for unsaturated ash-fall pyroclastic soils in the Campania region (southern Italy). Environ. Earth Sci. 67, 787–798. https://doi.org/10.1007/s12665-012-1531-4.

de Vita, S., Sansivero, F., Orsi, G., Marotta, E., Piochi, M., 2010. Volcanological and structural evolution of the island of Ischia (Italy) over the past 10 ka. In: Groppelli G, Viereck-Goette L (eds.) Stratigraphy and geology of volcanic areas. Geological Society of America, Special Paper 464, 193–241. https://doi.org/10.1130/2010.2464(10).

De Vita, P., Napolitano, E., Godt, J.W., Baum, R.L., 2013. Deterministic estimation of hydrological thresholds for shallow landslide initiation and slope stability models: case study from the Somma-Vesuvius area of southern Italy. Landslides 10, 713–728. https://doi.org/10.1007/s10346-012-0348-2.

de Vita, S., Sansivero, F., Orsi, G., Marotta, E., 2006. Cyclical slope instability and volcanism related to volcano-tectonism in resurgent calderas: The Ischia island (Italy) case study. Eng. Geol. 86, 148–165. https://doi.org/10.1016/j.enggeo.2006.02.013.

Del Prete, S., Mele, R., 1999. L'influenza dei fenomeni d'instabilità di versante nel quadro morfoevolutivo della costa dell'isola d'Ischia. Boll. Soc. Geol. It. 118, 339–360.

Del Prete, S., Mele, R., 2006. Il contributo delle informazioni storiche per la valutazione della propensione al dissesto nell'Isola d'Ischia. Rend. Soc. Geol. It. Nuova Serie 2, 29–47.

Della Seta, M., Marotta, E., Orsi, G., de Vita, S., Sansivero, F., Fredi, P., 2012. Slope instability induced by volcano-tectonics as an additional source of hazard in active volcanic areas: The case of Ischia island (Italy). Bull. Volcanol. 74, 79–106. https://doi.org/10.1007/s00445-011-0501-0.

Della Seta, M., Esposito, C., Marmoni, G.C., Martino, S., Paciello, A., Perinelli, C., Sottili, G., 2015. Geological constraints for a conceptual evolutionary model of the slope deformations affecting Mt. Nuovo at Ischia (Italy). Italian J. Eng. Geol. Environ. 2, 15–28. https://doi.org/10.4408/IJEGE.2015-02.O-02.

Di Maio, R., Piegari, E., Scotellaro, C., Soldovieri, M.G., 2007. Resistivity tomographies to define thickness and water content of pyroclastic covers at Mt. Di Vezzi (Ischia Island). Italian J. Eng. Geol. Environ. 2, 65–72. https://doi.org/10.4408/IJEGE.2007-02.O-05.

Di Maio, R., De Paola, C., Forte, G., Piegari, E., Pirone, M., Santo, A., Urciuoli, G., 2020. An integrated geological, geotechnical and geophysical approach to identify predisposing factors for flowslide occurrence. Eng. Geol. 267, 105473. https://doi.org/10.1016/j.enggeo.2019.105473.

Di Maio, R., Piegari, E., 2011. Water storage mapping of pyroclastic covers through electrical resistivity measurements. J. Appl. Geophys. 75, 196–202. https://doi.org/10.1016/j.jappgeo.2011.07.009.

Di Maio, R., Mauriello, P., Patella, D., Petrillo, Z., Piscitelli, S., Siniscalchi, A., 1998. Electric and electromagnetic outline of the Mount Somma-Vesuvius structural setting. J. Volcanol. Geoth. Res. 82 (1–4), 219–238. https://doi.org/10.1016/S0377-0273(97)00066-8.

Di Maio, R., Patella, D., Petrillo, Z., Siniscalchi, A., Cecere, G., De Martino, P., 2000. Application of electric and electromagnetic methods to the definition of the Campi Flegrei caldera (Italy). Ann. Geofis. 43 (2), 375–390. http://hdl.handle.net/2122/1286.

Dietrich, W., Montgomery, D., 1998. Shalstab: a digital terrain model for mapping shallow landslide potential, NCASI (National Council of the Paper Industry for Air and Stream Improvement) Technical Report, February, 26 p.

Donzelli, R., 1910. L'alluvione del 24 ottobre 1910 nell'isola d'Ischia e l'opera della squadra napoletana di soccorso. Tip. Lubrano, 301 p.

Forte, G., Pirone, M., Santo, A., Nicotera, M.V., Urciuoli, G., 2019. Triggering and predisposing factors for flow-like landslides in pyroclastic soils: the case study of the Lattari Mts. (southern Italy). Eng. Geol. 257, 105137. https://doi.org/10.1016/j.enggeo.2019.05.014.

Fusco, F., Allocca, V., De Vita, P., 2017. Hydro-geomorphological modelling of ash-fall pyroclastic soils for debris flow initiation and groundwater recharge in Campania (southern Italy). Catena 158, 235–249. https://doi.org/10.1016/j.catena.2017.07.010.

Fusco, F., De Vita, P., Mirus, B.B., Baum, R.L., Allocca, V., Tufano, R., Di Clemente, E., Calcaterra, D., 2019. Physically based estimation of rainfall thresholds triggering shallow landslides in volcanic slopes of southern Italy. Water 11 (9), 1915. https://doi.org/10.3390/w11091915.

Fusco, F., Mirus, B.B., Baum, R.L., Calcaterra, D., De Vita, P., 2021. Incorporating the effects of complex soil layering and thickness local variability into distributed landslide susceptibility assessments. Water 13, 713. https://doi.org/10.3390/w13050713.

Fusco, F., Bordoni, M., Tufano, R., Vivaldi, V., Meisina, C., Valentino, R., Bittelli, M., De Vita, P., 2022. Hydrological regimes in different slope environments and implications on rainfall thresholds triggering shallow landslides. Nat. Hazards 114, 907–939. https://doi.org/10.1007/s11069-022-05417-5.

Fusco, F., Tufano, R., De Vita, P., Di Martire, D., Di Napoli, M., Guerriero, L., Mileti, F.A., Terribile, F., Calcaterra, D., 2023. A revised landslide inventory of the Campania region (Italy). Sci. Data 10, 355. https://doi.org/10.1038/s41597-023-02155-6.
Gance, J., Malet, J.P., Supper, R., Sailhac, P., Ottowitz, D., Jochum, B., 2016. Permanent electrical resistivity measurements for monitoring water circulation in clayey landslides. J. Appl. Geophys. 126, 98–115. https://doi.org/10.1016/j.jappgeo.2016.01.011.
Giocoli, A., Stabile, T.A., Adurno, I., Perrone, A., Gallipoli, M.R., Gueguen, E., Norelli, E., Piscitelli, S., 2015. Geological and geophysical characterization of the southeastern side of the High Agri Valley (southern Apennines, Italy). Nat. Hazards Earth Syst. Sci. 15, 315–323. https://doi.org/10.5194/nhess-15-315-2015.
Glover, P.W.J., 2016. Archie's law – A reappraisal. Solid Earth 7, 1157–1169. https://doi.org/10.5194/se-7-1157-2016.
Greco, R., Comegna, L., Damiano, E., Guida, A., Olivares, L., Picarelli, L., 2013. Hydrological modelling of a slope covered with shallow pyroclastic deposits from field monitoring data. Hydrol. Earth Syst. Sci. 17 (10), 4001–4013. https://doi.org/10.5194/hess-17-4001-2013.
Greco, R., Marino, P., Bogaard, T.A., 2023. Recent advancements of landslide hydrology. WIREs Water 10, e1675. https://doi.org/10.1002/wat2.167.
Horton, R.E., 1933. The role of infiltration in the hydrologic cycle. Eos, Transactions American Geophysical Union 14 (1), 446–460.
Hungr, O., Leroueil, S., Picarelli, L., 2014. The Varnes classification of landslide types, an update. Landslides 11, 167–194. https://doi.org/10.1007/s10346-013-0436-y.
Jongmans, D., Garambois, S., 2007. Geophysical investigation of landslides: a review. Bull. Soc. Géol. France 178 (2), 101–112. https://doi.org/10.2113/gssgfbull.178.2.101.
Khan, M.A., Basharat, M., Riaz, M.T., Sarfraz, Y., Farooq, M., Khan, A.Y., Pham, Q.B., Ahmed, K.S., Shahzad, A., 2021. An integrated geotechnical and geophysical investigation of a catastrophic landslide in the Northeast Himalayas of Pakistan. Geol. J. 56 (9), 4760–4778. https://doi.org/10.1002/gj.4209.
Kiernan, M., Xuan, M., Montgomery, J., Anderson, J.B., 2022. Integrated characterization and analysis of a slow-moving landslide using geotechnical and geophysical methods. Geosciences 12 (11), 404. https://doi.org/10.3390/geosciences12110404.
Levinna, N., Jun, Y., 2024. New insights into the catastrophic slope failures at Sau Mau Ping: The role of antecedent rainfall pattern. Landslides 21 (7), 1501–1514. https://doi.org/10.1007/s10346-024-02247-3.
Liu, Y., Qiu, H., Kamp, U., Wang, N., Wang, J., Huang, C., Tang, B., 2024. Higher temperature sensitivity of retrogressive thaw slump activity in the Arctic compared to the Third Pole. Sci. Total Environ. 914 (2024), 170007. https://doi.org/10.1016/j.scitotenv.2024.170007.
Loke, M.H., Barker, R.D., 1996a. Practical techniques for 3D resistivity surveys and data inversion. Geophys. Prospect. 44, 499–523. https://doi.org/10.1111/j.1365-2478.1996.tb00162.x.
Loke, M.H., Barker, R.D., 1996b. Rapid least-squares inversion of apparent resistivity pseudosections by a quasi-Newton method. Geophys. Prospect. 44, 131–152. https://doi.org/10.1111/j.1365-2478.1996.tb00142.x.
Loke, M.H., Dahlin, T., 2002. A comparison of the Gauss-Newton and the quasi-Newton methods in resistivity imaging inversion. J. Appl. Geophys. 49, 149–162. https://doi.org/10.1016/S0926-9851(01)00106-9.
Loke, M.H., 2004. Tutorial: 2-D and 3-D Electrical Imaging Surveys. Geotomo Software, Res2dinv 3.5 Software, 136 p.
Lu, N., Godt, J.W., 2008. Infinite-slope stability under steady unsaturated seepage conditions. Water Resour. Res. 44, W11404. https://doi.org/10.1029/2008WR006976.
Lu, N., Godt, J.W., 2013. Hillslope Hydrology and Stability. Cambridge University Press, New York, NY, USA.
Lu, N., Likos, W.J., 2004. Unsaturated soil mechanics. Wiley, New York.
Marmoni, G.M., Martino, S., Heap, M.J., Reuschlé, T., 2017. Gravitational slope-deformation of a resurgent caldera: New insights from the mechanical behaviour of Mt. Nuovo tuffs (Ischia Island, Italy). J. Volcanol. Geoth. Res. 345, 1–20. https://doi.org/10.1016/j.jvolgeores.2017.07.019.
Massaro, L., Forte, G., De Falco, M., Rauseo, F., Santo, A., 2024. Rockfall source identification and trajectory analysis from UAV-based data in volcano-tectonic areas: a case study from Ischia Island, Southern Italy. Bulletin of Engineering Geology and the Environment 83 (3), 75. https://doi.org/10.1007/s10064-024-03569-1.
Mele, R., Del Prete, S., 1998. Fenomeni di instabilità dei versanti in Tufo Verde del Monte Epomeo (Isola d'Ischia—Campania). Boll. Soc. Geol. Ital. 117, 93–112.
Napolitano, E., Fusco, F., Baum, R.L., Godt, J.W., De Vita, P., 2016. Effect of antecedent-hydrological conditions on rainfall triggering of debris flows in ash-fall pyroclastic mantled slopes of Campania (southern Italy). Landslides 13, 967–983. https://doi.org/10.1007/s10346-015-0647-5.
Orsi, G., Piochi, M., Campajola, L., D'Onofrio, A., Gialanella, L., Terrasi, F., 1996. ^{14}C geochronological constraints for the volcanic history of the island of Ischia (Italy) over the last 5000 years. J. Volcanol. Geoth. Res. 71, 249–257. https://doi.org/10.1016/0377-0273(95)00067-4.
Papadopoulos, N.G., Yi, M.J., Kim, J.H., Tsourlos, P., Tsokas, G.N., 2010. Geophysical investigation of tumuli by means of surface 3D Electrical Resistivity Tomography. J. Appl. Geophys. 70 (3), 192–205. https://doi.org/10.1016/j.jappgeo.2009.12.001.
Park, H.J., Lee, J.H., Woo, I., 2013. Assessment of rainfall-induced shallow landslide susceptibility using a GIS-based probabilistic approach. Eng. Geol. 161, 1–15. https://doi.org/10.1016/j.enggeo.2013.04.011.
Pasierb, B., Grodecki, M., Gwóźdź, R., 2019. Geophysical and geotechnical approach to a landslide stability assessment: a case study. Acta Geophys. 67, 1823–1834. https://doi.org/10.1007/s11600-019-00338-7.
Patella, D., 1997. Self-potential global tomography including topographic effects. Geophys. Prospect. 45 (5), 843–863. https://doi.org/10.1046/j.1365-2478.1997.570296.x.
Pazzi, V., Morelli, S., Riccardo, F., 2019. A Review of the Advantages and Limitations of Geophysical Investigations in Landslide Studies. Int. J. Geophys. 2019, 1–27. https://doi.org/10.1155/2019/2983087.
Perrone, A., Lapenna, V., Piscitelli, S., 2014. Electrical resistivity tomography technique for landslide investigation: A review. Earth Sci. Rev. 135, 65–82. https://doi.org/10.1016/j.earscirev.
Philip, J.R., 1957. The theory of infiltration: 1. The infiltration equation and its solution. Soil Sci. 83, 345–357.
Pirone, M., Di Maio, R., Forte, G., De Paola, C., Di Marino, E., Salone, R., Santo, A., Urciuoli, G., 2023. Study of the groundwater regime in unsaturated slopes prone to landslides by multidisciplinary investigations: Experimental study and numerical modelling. Eng. Geol. 315, 107045. https://doi.org/10.1016/j.enggeo.2023.107045.
Prancevic, J.P., Lamb, M.P., McArdell, B.W., Rickli, C., Kirchner, J.W., 2020. Decreasing landslide erosion on steeper slopes in soil-mantled landscapes. Geophys. Res. Lett. 47, e2020GL087505. https://doi.org/10.1029/2020GL087505.
Ren, D., Fu, R., Leslie, L.M., Dickinson, R., Xin, X., 2010. A stormtriggered landslide monitoring and prediction system: Formulation and case study. Earth Interact 14, 1–24. https://doi.org/10.1175/2010EI337.1.
Revil, A., Jardani, A., 2013. The Self-Potential Method. Theory and Applications in Environmental Geosciences. Cambridge Univ. Press, Cambridge, 369 p.
Revil, A., Naudet, V., Nouzaret, J., Pessel, M., 2003. Principles of electrography applied to self-potential electrokinetic sources and hydrogeological applications. Water Resour. Res. 39, 1114. https://doi.org/10.1029/2001WR000916.
Reynolds, W.D., Elrick, D.E., 1986. A method for simultaneous in-situ measurement in the vadose zone of field-saturated hydraulic conductivity, sorptivity, and the conductivity-pressure head relationship. Ground Water Monit. Rev. 6, 84–95.
Rianna, G., Reder, A., Pagano, L., 2023. From empirically to physically based early warning predictions of rainfall-induced landslides in silty volcanic soils: the Lattari Mountains case study. Bulletin of Engineering Geology and the Environment 82 (6), 223.
Romeo, S., D'Angiò, D., Fraccica, A., Licata, V., Vitale, V., Chiessi, V., Amanti, M., Bonasera, M., 2023. Investigation and preliminary assessment of the Casamicciola landslide in the island of Ischia (Italy) on November 26, 2022. Landslides 20, 1265–1276. https://doi.org/10.1007/s10346-023-02064-0.
Rossi, G., Catani, F., Leoni, L., Segoni, S., Tofani, V., 2013. HIRESSS: a physically based slope stability simulator for HPC applications. Nat. Hazards Earth Syst. Sci. 13, 151–166. https://doi.org/10.5194/nhess-13-151-2013.
Salciarini, D., Tamagnini, C., Conversini, P., Rapinesi, S., 2012. Spatially distributed rainfall thresholds for the initiation of shallow landslides. Nat. Hazards 61, 229–245. https://doi.org/10.1007/s11069-011-9739-2.
Salciarini, D., Fanelli, G., Tamagnini, C., 2017. A probabilistic model for rainfall-induced shallow landslide prediction at the regional scale. Landslides 14, 1731–1746. https://doi.org/10.1007/s10346-017-0812-0.
Salvatici, T., Tofani, V., Rossi, G., D'Ambrosio, M., Tacconi, S.C., Masi, E.B., Rosi, A., Pazzi, V., Vannocci, P., Petrolo, M., Catani, F., Ratto, S., Stevenin, H., Casagli, N., 2018. Application of a physically based model to forecast shallow landslides at a regional scale. Nat. Hazards Earth Syst. Sci. 18, 1919–1935. https://doi.org/10.5194/nhess-18-1919-2018.
Sanglerat, G., 1972. The Penetrometer and Soil Exploration. Developments in Geotechnical Engineering 1. Elsevier Publishing: New York. ISBN 978-0444565952, 488 p.
Santo, A., Di Crescenzo, G., Del Prete, S., Di Iorio, L., 2012. The Ischia island flash flood of November 2009 (Italy): Phenomenon analysis and flood hazard. Phys. Chem. Earth 49, 3–17. https://doi.org/10.1016/j.pce.2011.12.004.
Saxton, K.E., Willey, P.H., 2006. The SPAW model for agricultural field and pond hydrologic simulation. Chapter 17. In: Singh V.P., Frevert D. (eds.) Mathematical modeling of watershed hydrology. CRC Press, ISBN 9780429122446, 678 p.
Saxton, K.E., Rawls, W.J., 2006. Soil water characteristic estimates by texture and organic matter for hydrologic solutions. Soil Sci. Soc. Am. J. 70, 1569–1578.
Selva, J., Acocella, V., Bisson, M., Caliro, S., Costa, A., Della Seta, M., De Martino, P., de Vita, S., Federico, C., Giordano, G., Martino, S., Cardaci, C., 2019. Multiple natural hazards at volcanic islands: a review for the Ischia volcano (Italy). J. Appl. Volcanol. 8, 5. https://doi.org/10.1186/s13617-019-0086-4.
Sepe, C., Calcaterra, D., Di Martire, D., Fusco, F., Tufano, R., Vitale, E., Guerriero, L., 2023. Triggering conditions and propagation of the December 2019 Palma Campania landslide: Implications for residual hazard estimation at recurrent landslide sites. Eng. Geol. 322, 107177. https://doi.org/10.1016/j.enggeo.2023.107177.
Sharma, P.S., 1997. Environmental and Engineering Geophysics. Cambridge Univ. Press, ISBN 9781139171168, 499p.
Sidle, R.C., Ochiai, H., 2006. Landslides: processes, prediction, and land use. American Geophysical Union, Washington, D.C., USA. ISBN 9780875903224, 312 p.
Simoni, S., Zanotti, F., Bertoldi, G., Rigon, R., 2008. Modelling the probability of occurrence of shallow landslides and channelized debris flows using GEOtop-FS. Hydrol. Process. 22, 532–545. https://doi.org/10.1002/hyp.6886.
Soueid Ahmed, A., Jardani, A., Revil, A., Dupont, J.P., 2016. Joint inversion of hydraulic head and self-potential data associated with harmonic pumping tests. Water Resour. Res. 52, 6769–6791. https://doi.org/10.1002/2016WR019058.
Soil Science Division Staff, 2017. Soil survey manual. C. Ditzler, K. Scheffe, and H.C. Monger (eds.). USDA Handbook 18. Government Printing Office, Washington, D.C., 639 p.

Sujitapan, C., Kendall, M., Whiteley, J.S., Chambers, J.E., Uhlemann, S., 2019. Landslide investigation and monitoring using self-potential methods. Proceedings 25th European Meeting of Environmental and Engineering Geophysics. Near Surface Geoscience Conference and Exhibition 2019, NSG 2019. https://doi.org/10.3997/2214-4609.201902428.

Taylor, S.B., Barker, R.D., 2002. Resistivity of partially saturated Triassic Sandstone. Geophys. Prospect. 50, 603–613. https://doi.org/10.1046/j.1365-2478.2002.00339.x.

Thirard, G., Grandjean, G., Thiery, Y., Maquaire, O., François, B., Lissak, C., Costa, S., 2020. Hydrogeological assessment of a deep-seated coastal landslide based on a multi-disciplinary approach. Geomorphology 371, 107440. https://doi.org/10.1016/j.geomorph.2020.107440.

Tofani, V., Bicocchi, G., Rossi, G., Segoni, S., D'Ambrosio, M., Casagli, N., Catani, F., 2017. Soil characterization for shallow landslides modeling: a case study in the Northern Apennines (Central Italy). Landslides 14, 755–770. https://doi.org/10.1007/s10346-017-0809-8.

Tufano, R., Formetta, G., Calcaterra, D., De Vita, P., 2021. Hydrological control of soil thickness spatial variability on the initiation of rainfall-induced shallow landslides using a three-dimensional model. Landslides 18, 3367–3380. https://doi.org/10.1007/s10346-021-01681-x.

USDA, 2022. Keys to soil taxonomy. USDA-Nat, Res. Cons. Service, 13th ed., 410 p.

van Genuchten, M.T., 1980. A closed form equation for predicting the hydraulic conductivity of unsaturated soils. Soil Sci. Soc. Am. J. 44, 892–898.

van Genuchten, M.T., Simunek, J., Leij, F.J., Sjna, M., 1994. RETC Code for quantifying the hydraulic functions of unsaturated soils. Salinity Laboratory USDA, Riverside, 93 p.

Vezzoli, L., 1988. The island of Ischia. CNR Quaderni de "La Ricerca Scientifica" 114, 1–122, Roma, Italia, 133 p.

Ye, B., Qiu, H., Tang, B., Liu, Y., Liu, Z., Jiang, X., Yang, D., Ullah, M., Zhu, Y., Kamp, U., 2024. Creep deformation monitoring of landslides in a reservoir area. J. Hydrol. 632, 130905. https://doi.org/10.1016/j.jhydrol.2024.130905.

Zangar, C.N., 1953. Theory and problems of water percolation. U.S. Bureau Engineering Monograph, 8. U.S. Bureau of Reclamation Denver, CO. 86 p.

Zarroca, M., Linares, R., Roqué, C., Rosell, J., Gutiérrez, F., 2014. Integrated geophysical and morphostratigraphic approach to investigate a coseismic (?) translational slide responsible for the destruction of the Montclús village (Spanish Pyrenees). Landslides 11, 655–671. https://doi.org/10.1007/s10346-013-0427-z.

Zhang, F., Peng, J., Wu, X., Pan, F., Jiang, Y., Kang, C., Wu, W., Ma, W., 2021. A catastrophic flowslide that overrides a liquefied substrate: the 1983 Saleshan landslide in China. Earth Surf. Process. Landforms 46, 2060–2078. https://doi.org/10.1002/esp.5144.